UPPSALA
UNIVERSITET

Digital Comprehensive Summaries of Uppsala Dissertations from the Faculty of Science and Technology 635

The Rôle of Side-Chains in Polymer Electrolytes for Batteries and Fuel Cells

JAANUS KARO

ACTA
UNIVERSITATIS
UPSALIENSIS
UPPSALA
2009

ISSN 1651-6214
ISBN 978-91-554-7499-7
urn:nbn:se:uu:diva-100738

Dissertation presented at Uppsala University to be publicly examined in Häggsalen, Ångströmlaboratoriet, Lägerhyddsvägen 1, Uppsala, Monday, May 11, 2009 at 10:15 for the degree of Doctor of Philosophy. The examination will be conducted in English.

Abstract
Karo, J. 2009. The Rôle of Side-Chains in Polymer Electrolytes for Batteries and Fuel Cells. Acta Universitatis Upsaliensis. *Digital Comprehensive Summaries of Uppsala Dissertations from the Faculty of Science and Technology* 635. 51 pp. Uppsala. ISBN 978-91-554-7499-7.

The subject of this thesis relates to the design of new polymer electrolytes for battery and fuel cell applications. Classical Molecular Dynamics (MD) modelling studies are reported of the nano-structure and the local structure and dynamics for two types of polymer electrolyte host: poly(ethylene oxide) (PEO) for lithium batteries and perfluorosulfonic acid (PFSA) for polymer-based fuel cells. Both polymers have been modified by side-chain substitution, and the effect of this on charge-carrier transport has been investigated. The PEO system contains a 89-343 EO-unit backbone with 3-15 EO-unit side-chains, separated by 5-50 EO backbone units, for $LiPF_6$ salt concentrations corresponding to Li:EO ratios of 1:10 and 1:30; the PFSA systems correspond to commercial Nafion®, Hyflon® (Dow®) and Aciplex® fuel-cell membranes, where the major differences again lie in the side-chain lengths.

The PEO mobility is clearly enhanced by the introduction of side-chains, but is decreased on insertion of Li salts; mobilities differ by a factor of 2-3. At the higher Li concentration, many short side-chains (3-5 EO-units) give the highest ion mobility, while the mobility was greatest for side-chain lengths of 7-9 EO units at the lower concentration. A picture emerges of optimal Li^+-ion mobility correlating with an optimal number of Li^+ ions in the vicinity of mobile polymer segments, yet not involved in significant cross-linkages within the polymer host.

Mobility in the PFSA-systems is promoted by higher water content. The influence of different side-chain lengths on local structure was minor, with Hyflon® displaying a somewhat lower degree of phase separation than Nafion®. Furthermore, the velocities of the water molecules and hydronium ions increase steadily from the polymer backbone/water interface towards the centre of the proton-conducting water channels. Because of its shorter side-chain length, the number of hydronium ions in the water channels is ~50% higher in Hyflon® than in Nafion® beyond the sulphonate end-groups; their hydronium-ion velocities are also ~10% higher.

MD simulation has thus been shown to be a valuable tool to achieve better understanding of how to promote charge-carrier transport in polymer electrolyte hosts. Side-chains are shown to play a fundamental rôle in promoting local dynamics and influencing the nano-structure of these materials.

Keywords: molecular dynamics, polymer electrolytes, side-chains, Li-ion batteries, proton exchange membrane fuel cell (PEMFC), PFSA membrane

Jaanus Karo, Department of Materials Chemistry, Structural Chemistry, Box 538, Uppsala University, SE-75121 Uppsala, Sweden, Department of Physics and Materials Science, Atomic and molecular physics, Box 530, Uppsala University, SE-75121 Uppsala, Sweden

ISSN 1651-6214
ISBN 978-91-554-7499-7
urn:nbn:se:uu:diva-100738 (http://urn.kb.se/resolve?urn=urn:nbn:se:uu:diva-100738)

List of papers

Paper **I**: **A molecular dynamics study of the effect of side-chains on mobility in a polymer host**
J. Karo, A. Aabloo and J.O. Thomas, *Solid State Ionics*, **176** (2005) 3041-3044

Paper **II**: **A molecular dynamics study of the influence of side-chain length and spacing on lithium mobility in non-crystalline $LiPF_6 \cdot PEO_x$; x=10 and 30**
J. Karo and D. Brandell, submitted to *Solid State Ionics*

Paper **III**: **Molecular dynamics studies of the Nafion®, Dow® and Aciplex® fuel-cell polymer membrane systems**
D. Brandell, J. Karo, A. Liivat and J.O. Thomas, *Journal of Molecular Modeling,* **13** (2007) 1039–1046

Paper **IV**: **Molecular dynamics modelling of proton transport in Nafion® and Hyflon® nano-structures**
J. Karo, A. Aabloo, J.O. Thomas and D. Brandell, submitted to *Journal of Physical Chemistry, B.*

Comments on my contribution to this work:

Papers I, II, IV: The majority of the work in all its phases: model preparation, simulation, data analysis and manuscript writing.
Paper III: A significant part of the project planning and the vast majority of the analysis phase.
Thesis: I was helped with the translation of the *Populärvetenskaplig Sammanfattning* into Swedish by my supervisor Dr. Daniel Brandell.

Other published papers not included in this work:

Application of the Monte Carlo method for creation of initial models of EAP molecules for Molecular Dynamics simulation
E. Soolo, J. Karo, H. Kasemägi, M. Kruusmaa and A. Aabloo, *Proc. SPIE*, **6168** (2006), 61682A-12

Contents

Introduction 7
- Li batteries - electrical energy storage 7
- PEM fuel-cells - electrical energy conversion 9
- Polymer electrolytes 11
  - LiX·PEO electrolytes 11
  - PFSA membranes 12
- Computer simulation 14
- The effect of side-chains 15

Molecular Dynamics simulation 16
- Overview 16
- The force-field detail 16
- Initial structures and simulation detail 17
- Analysis 19

PEO-based materials 22
- Structure 22
  - Polymer structure 22
  - Ion distribution 22
  - Cross-linkage 24
- Mobility 25
  - Polymer mobility 25
  - Ion mobility 27
  - Diffusion 29
  - Ion-jump mechanism 29

PFSA-based materials 32
- Local structure 32
- Nano-scale structure 36
- Dynamics 39
  - Mobility 39
  - Diffusion coefficients 41

Concluding remarks 42

Populärvetenskaplig sammanfattning 44

Acknowledgements 46

References 47

Appendix 50

Abbreviations

CNF	Coordination Number Function
DFT	Density Functional Theory
EO	Ethylene Oxide
EVB	Empirical Valence-Bond
EW	Equivalent Weight
FC	Fuel Cell
FF	Force-Field
LSC	Long Side-Chain
MD	Molecular Dynamics
MEA	Membrane Electrode Assembly
MRT	Mean Residence Time
MSD	Mean-Square-Displacement
MS-EVB	MultiState Empirical Valence-Bond
PEMFC	Proton Exchange Membrane Fuel Cell
PEO	Poly(Ethylene Oxide)
PFSA	PerFluoroSulfonic Acid
PFSI	PerFluoroSulfonate Ionomer
PTFE	PolyTetraFluoroEthylene
QENS	Quasi-Elastic Neutron Scattering
RDF	Radial Distribution Function
SANS	Small-Angle Neutron Scattering
SAR	Structure-Activity Relationship
SAVR	Surface Area to Volume Ratio
SAXS	Small-Angle X-ray Scattering
SC	Side-Chain
SHE	Standard Hydrogen Electrode
SSC	Short Side-Chain
TFSI	*bis*-(TriFluoromethylSulphonyl)Imide
WAXD	Wide-Angle X-ray Diffraction

Introduction

Global energy consumption is constantly increasing, not least in countries like China and India, which currently experience rapid economic growth rate. Although more and more attention is directed towards renewable and environmentally friendly energy production methods, conventional fossil fuels are still our primary energy sources. These sources, however, give rise to pollution in the form of greenhouse gases, and there is also a growing fear that the global oil reserves are becoming critically small to meet the increasing demand for energy. These problems force us to search for and develop alternative energy sources.

Electrical energy is both a convenient and universal form of energy, widely used in the world today. At the moment, almost 17 % of the world's total energy consumption is electrical energy [1]. Electrical energy is produced from a number of different sources: fossil fuels, nuclear power, solar power, wind, hydroelectric power, geothermal heat, *etc*. However, many of the environmentally friendly sources of electrical energy cannot operate at all times, and the energy produced thus needs to be instantly consumed. Furthermore, not all applications which need energy can be connected to the power grid. Hence, a need for electrical energy storage exists. Today, much of this storage is done in rechargeable batteries and supercapacitors. Alternatively, energy conversion can be achieved in fuel cells, but these storage methods have so far only been used to a minor degree in the energy system.

Battery and fuel-cell technologies therefore need further development to work efficiently and store more energy. In this context, this thesis treats polymer electrolytes for use in batteries and fuel cells.

Li batteries - electrical energy storage

A lithium battery is an electrochemical device comprising a negative electrode (anode), an electrolyte and a positive electrode (cathode), with lithium as the mobile ion in the system. In all modern rechargeable Li-ion batteries, the electrode materials are intercalation materials. Upon charging, lithium ions deintercalate from the layered intercalation host (cathode), travel across the electrolyte, and become intercalated into the anode. When the battery discharges, this process is reversed. At the same time as ions travels across the battery, electrons pass around an external circuit and thereby supply electrical energy. Interest in the alkali metal lithium has arisen from two of its

unique properties: it is the most electronegative metal (~ -3.0 V *vs.* SHE), and it is the lightest of the metals (0.534 g cm^{-3}). These properties give a high energy content per unit weight.

Lithium battery technology has been developed during the past thirty years. The first interest in lithium batteries began with the work of Harris in 1958 [2] which led to the development of *primary lithium cells* (*i.e.,* non-rechargeable batteries) in the 1970s. The more prominent systems at the time included lithium/sulfurdioxide (Li/SO_2), lithium thionylchloride ($Li/SOCl_2$), lithium sulfurylchloride (Li/SO_2Cl_2), lithium polycarbon monofluoride ($Li/(CF_x)_n$)) and lithium manganesedioxide (Li/MnO_2) [3]. However, explosions occurred due to lithium dendrite growth and high reactivity of the metallic anode.

Studies of fast ion conduction in solids demonstrated that alkali metal ions could move rapidly in an electronically conducting lattice containing transition metal atoms in a mixed valence state [3]. This led to the development of *rechargeable lithium batteries* during the late 1970s and 1980s, using lithium intercalation compounds as positive electrodes. The first systems, operating at low voltage, were Li/TiS_2 and Li/MoS_2. These systems continued to use metallic lithium anodes, so the safety problems due to dendrite growth limited their commercial application. Steele considered the use of insertion compounds also as battery anodes, and suggested graphite and layered sulfides as potential candidates for electrodes in a lithium-ion battery based on a non-aqueous liquid electrolyte [4]. A lithium-ion cell was tested in the laboratory with two insertion electrodes cycling lithium ions between them, thus eliminating the use of a metallic lithium anode [5,6]. Eventually, in 1991, Sony introduced the first commercial Li-ion battery based on $C/LiCoO_2$. The cells had an operational voltage of 3.6 V.

Today, Li-ion polymer batteries are lightweight, produce high voltages and are very common in our everyday lives, for example, in mobile phones, laptops, media-players, *etc*. The battery has a high energy-density, but is unfortunately a low power-device (slow charge/discharge) because of the low intrinsic diffusivity of the lithium ion in the solid state (ca. 10^{-8} cm^2s^{-1}), which limits the rate of intercalation/deintercalation, and hence of charge/discharge.

A related problem is the similarly low lithium ion diffusion in solid state electrolytes. Current Li-ion battery development focuses on non-liquid electrolytes, in particular polymer electrolytes. Such batteries are expected to be less expensive and more easily scaled up than their liquid-based counterparts, allowing packing in light-weight plastic containers with any desired shape or size. Also – and perhaps more importantly – ionically conducting solid materials are safer than liquid electrolytes, free from problems with leakage of harmful liquids or degassing. The flexibility of polymeric materials allows volume changes upon intercalation/deintercalation to be accommodated.

Many lithium-ion conducting polymer electrolytes for batteries have been prepared and characterized. However, the greatest attention has undoubtedly been directed towards poly(ethylene oxide)-based (PEO-based) solid polymer electrolytes. PEO has a number of appealing features, such as low cost, good chemical stability, safety and ability to form any shape. However, there are also problems associated with the PEO-based materials. Their conductivity is high only at temperatures exceeding 70 ºC. At room temperature, the conductivity in pure and unmodified PEO-based electrolytes reaches only 10^{-8} S cm^{-1} [7], which is insufficient for most lithium battery applications. In addition, the conductivity is dominated by the anions, which may result in concentration polarization, limiting the rate (power) of the battery.

Some important attempts to improve ionic conductivity in Li-ion batteries have been made, mainly by suppressing crystallinity and increasing the amorphous phase content. Examples include adding cross-links, plasticisers [8], inorganic nanoparticles [9] and side-chains [10-12]. Another way to improve ion conductivity is to stretch the material mechanically to increase polymer chain order by unravelling loops in the polymer molecules [13]. However, the conductivity of solid state electrolytes is still considered too low for most applications.

PEM fuel-cells - electrical energy conversion

A Fuel Cell (FC) is an electrochemical converter – chemical energy in the fuel (hydrogen or another hydrogen source such as methanol) is converted into electrical energy. FC efficiency is higher than in conventional combustion engines [14,15]. In the near future, FCs might become one of the most important energy conversion devices, supplementing or even substituting conventional fossil fuel combustion engines. The first working demonstration of a fuel cell was performed by William Grove in 1839 [16] in an experiment where water was electrolysed into hydrogen and oxygen by passing through it an electric current. Current was generated by reversing the process.

There exists a range of different types of FC today, some smaller and portable, some larger and suitable for power stations. However, due to problems with high prices and the relatively short lifetime of the materials, FCs are not yet so common in everyday life.

A Proton Exchange Membrane Fuel Cell (PEMFC) consists of several components: electrodes and gas diffusion layers separated by a proton exchange membrane, a fuel supply system, fuel flow plates, a cooling system and a control system. The basic components of a PEMFC are seen in Figure 1. The main principle is simple: hydrogen fuel and air oxygen are consumed in the overall reaction: $2\ H_2 + O_2 \rightarrow 2\ H_2O$. At the anode, the hydrogen gas ionizes, releasing electrons and creating protons: $2\ H_2 \rightarrow 4\ H^+ + 4\ e^-$. On the cathode side, oxygen reacts with electrons supplied by the electrode and H^+ ions from the electrolyte to form water: $O_2 + 4\ e^- + 4\ H^+ \rightarrow 2H_2O$, in a reac-

tion which generates electricity. The only emission from the device is water. There are other types of fuel or 'hydrogen-carriers' for FC systems, such as methane, ammonia, methanol, ethanol, etc. [15].

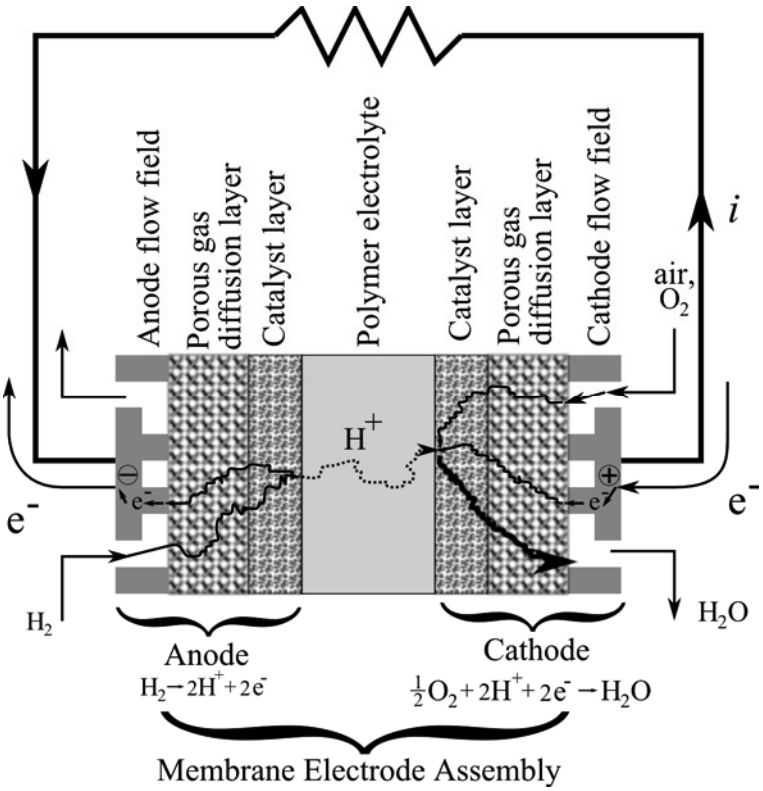

Figure 1. Basic components and function of a PEMFC.

The Membrane Electrode Assembly (MEA) is the heart of the fuel cell, and perhaps the most critical component in enhancing FC performance. This thesis focuses on the Proton Exchange Membrane (PEM) part of the MEA, which constitutes the most common type of low temperature FC. The material in a PEM must satisfy tough demands: it has to have high intrinsic proton conductivity; good mechanical properties; chemically and electrochemically stable in an acidic and oxidizing environment; and low permeability for the fuel (gas or liquid).

PEMFCs require the use of liquid water since they rely on the proton transport across the membrane [17]. Water is transported into the FC as part of the reactant mixture, but is also a product of the overall reaction. It exists in liquid form in the PEM and is also mixed with the gaseous reactants which flow through the electrodes and flow plates in the fuel cell. The transport of water through the electrolyte is driven by diffusion, electro-osmotic effects, pressure gradients, and electrochemical reactions. Without sufficient water in the polymer electrolyte and catalyst layers, proton transport and

electrode reactivity are poor. Excess liquid water at the catalyst and porous transport layers, however, hinders reactant transport, and the water can solidify into ice at low temperatures. It is therefore important in FC design to maintain a proper water balance.

Perfluorosulfonic acid (PFSA)- or perfluorosulfonate ionomer (PFSI)-based polymer membranes are the most commonly used in PEM fuel cells, and have been studied for several decades. They are graft polymers, consisting of backbones of polytetrafluoroethylene (PTFE; $-(CF_2)_n-$) and have side-chains terminated by $-SO_3H$ end-groups. They differ mainly in side-chain length and equivalent weight (EW). EW is defined as the dry ionomer weight per mole of sulfonic acid group. A higher EW can correspond to longer side-chains and/or longer side-chain separation. This typically results in a higher formation of semi-crystalline regions in the PFSA material [18], which has a strong positive influence on its mechanical properties.

Nafion®, developed by DuPont in the mid-1960s, is the most widely used and well-known PFSA material [18-21]. Besides Nafion®, several other PFSA materials have been studied: Flemion® [22-24] and Aciplex® [23] from Asahi Glass, and the short side-chain (SSC) PFSA membrane Hyflon®, originally synthesized by the Dow Chemical Company, but more recently by Solvay-Solexis [25-30].

Polymer electrolytes

LiX·PEO electrolytes

The very first and still most studied solvent-free polymer electrolyte for batteries was based on high molecular weight poly(ethylene oxide), PEO $-(CH_2CH_2O)_n-$ [31], which remains the basis for almost all solvent-free polymer electrolyte systems. Since PEO materials are not brittle, they are able to form good interfacial contacts with the electrode materials and, more importantly, maintain contact under the stress caused by volume changes associated with cell charging and discharging. PEO also satisfies other demands, such as having low electronic conductivity, good mechanical properties, chemical stability and ease of processing.

In the 1970s, the basic structure of PEO-LiX polymer electrolytes was envisaged as long PEO chain helices wrapped around Li^+ cations to give a tunnel-type structure separating the cations from the X^- counterions [8]. Later, crystal structure determinations confirmed this to be correct for the crystalline polymer-salt complexes, but the actual arrangement of PEO is highly dependent on the PEO/salt concentration ratio [32,33].

An ideal ionic conductivity for a lithium-ion polymer electrolyte is accepted to be above 10^{-2}-10^{-3} Scm^{-1} but, despite much effort to modify pure PEO, the level of conductivity still does not exceed 10^{-4} Scm^{-1} at room temperature. In this context, it has been identified as a problem that pure PEO at

ambient conditions crystallize to a high degree – 75-80% – since these phases are generally considered to be isolating. Studies [34] have shown that above the melting point of pure PEO (65 ºC), a crystalline phase and a more dilute amorphous phase co-existed, with the latter being responsible for the fast ionic transport. As temperature is increased, the crystalline phase gradually dissolves into the amorphous phase. Therefore, research has been directed towards suppressing crystallinity at lower temperatures.

Anions, in particular large ones, have a major influence on the phase composition and crystallinity, weakening the interaction between the chains and reducing their ability to pack into a regular structure. This results in a lower melting point for the crystalline phase. For instance, a mixture of PEO-LiTFSI is completely amorphous for EO:Li salt-concentration ratios between 8:1 and 10:1, and semi-crystalline above 10:1 [8]. Another way to suppress crystallinity is to modify PEO structurally, for example, by adding side-chains. To better understand the effect of the presence of side-chains is the main purpose of this thesis.

Ion mobility in a PEO-based electrolyte is considered to be promoted by the local segmental motion of the polymer chains, by forming and breaking coordination between Li^+ and the EO atoms of polymer, and thereby providing free volume into which the ion can diffuse under the influence of an electric field. Side-chains can also undergo local segmental chain motion. Watanabe and co-workers were the first in this context to synthesize comb-polymer hosts with both backbone and side-chains containing EO units [10,12,35,36]. They could show that ionic conductivity was coupled to side-chain motion, and that the conductivity of $LiClO_4$-PEO and LiTFSI-PEO solutions could be raised by more than one order of magnitude by inserting methyl-group terminated side-chains with lengths up to 3 EO units [35]. The conductivity also increased for LiTFSI and $LiClO_4$ salts when the side-chain spacing of this comb-PEO was decreased [37,38], achieving conductivities of $1.5 \cdot 10^{-4}$ and $1.4 \cdot 10^{-3}$ Scm^{-1} at 30 and 80 °C, respectively [37].

To further explore the relationship between ion mobility and PEO side-chains, one of the goals behind this thesis is to systematically vary the side-chain configuration. A set of computer simulations have been prepared containing several PEO systems, constructed with different side-chain lengths and separations. In that the simulation conditions were the same for all systems studied, the variation of the polymer side-chains could be investigated.

PFSA membranes

Many papers have been published examining morphological properties in different PFSA materials, mostly using experimental techniques such as small-angle X-ray scattering (SAXS), small-angle neutron scattering (SANS) or wide-angle X-ray diffraction (WAXD) [27,39]. Hitherto, these investigations have not reached any consensus model for understanding the structures of these materials. Instead, several models have been introduced.

Their common feature is that there exist a phase separation between the hydrophobic backbones and hydrophilic sulfonic-acid terminated side-chains which are located in water clusters. The size and shape of the hydrophilic clusters are strongly dependent on the water content in the material. The most thoroughly discussed structure model is perhaps that suggested by Gierke [40]; the so called cluster-network model. It consists of an equal distribution of sulfonate ion clusters with ~40 Å diameter, held within a continuous fluorocarbon lattice. Narrow channels about 10 Å in diameter interconnect these clusters. However, Schmidt-Rohr and Chen recently suggested a completely new structural model [41]. They claim that long parallel but otherwise randomly packed water channels are surrounded by partially hydrophilic side branches, forming inverted-micelle cylinders. At 20 vol% water, the water channels are supposed to have diameters of on average 2.4 nm. Furthermore, Schmidt-Rohr and Chen claim that the Nafion semi-crystallites (~10 vol%), forming physical cross-links which are crucial for the mechanical properties of the Nafion films, are elongated and parallel to the water channels with cross-sections of ~5 $(nm)^2$.

For decades, Nafion has been considered as the best choice as PEM for FCs. However, recently published papers show good performances for short side-chain (SSC) types of PFSA, and suggest these as a replacement for Nafion® [25,42,43,44], not least because of their higher glass transition temperatures. It is well known that increasing the working temperature in an FC would increase its performance. This would increase the reaction rates at the catalysts, reduce the CO poisoning on the catalyst layers and avoid the degradation of the polymer membrane by hydrogen peroxide [45]. The glass transition temperature in Nafion has been measured to T_g = 110 °C, while Hyflon has been reported to have T_g around 165 °C. Above T_g, Nafion 117 starts to show plastic deformation due to the loss of physical cross-links and the degrading contact between electrolyte and electrodes [43]. Furthermore, SSC ionomers, as a consequence of their lower molecular-weight pendant group, show a semi-crystallinity content that is higher than the correspondent long side-chain (LSC) ionomers of the same EW [42]. Therefore, lower-EW membranes, *i.e.*, membranes with higher ionic content, can be prepared with the same semi-crystallinity if a SSC is used instead of a LSC. Alternatively, if the SSC and LSC membranes have similar EW values, the SSC is likely to have a higher content of semi-crystalline regions, *i.e.*, better mechanical properties.

Despite all the attention PFSA-based materials have received in industry and in the academic world, the exact structure of the membrane remains unknown and, as a result, the mechanisms of the electrochemical reactions during fuel-cell operation are not well understood. Many important issues still need to be treated further for this class of membrane material: the protonic conductivity needs to be enhanced, fuel cross-over needs to be decreased, the electro-osmotic drag of water needs to be lowered. In this thesis, the Molecular Dynamics (MD) simulation method has been used to shed light on some of these fundamental questions.

Computer simulation

The first computer simulations of materials were performed more than 50 years ago. Computational power has since increased to a level where computational chemistry is possible to supplement experiment, and provide an alternative "window" into the microscopic world [46-48]. The exciting part of modelling molecular systems is its multidisciplinary character: biologists describe the cellular picture; chemists address the atomic and molecular detail; physicists expand this view to the electronic level and probe underlying forces; mathematicians construct numerical models and algorithms; and computer scientists implement all these ideas and models into a computer programs. The computational techniques cover first principle *ab inito* and semi-empirical quantum mechanics, empirical (molecular) mechanics, molecular dynamics, Monte Carlo, free energy and solvation methods, structure-activity relationships (SAR) and many more methodologies. Modelling approaches supplement our knowledge extracted from experimental data and fill in many gaps in our understanding. Therefore, they are useful to develop better models and theories that will ultimately make predictions of material behaviour.

When studying the effect of side-chains in polymer electrolytes, there are different modelling techniques for different purposes. There exists for example a number of papers using quantum mechanics, in which the role of side-chains in the proton transfer of PFSA membranes [49,50] has been studied, but these studies are on comparatively small systems since the technique is computationally expensive. Using Molecular Dynamics (MD) methodology, however, several thousands of atoms can be considered simultaneously. There are already a limited number of groups who have used classical MD techniques for modelling Nafion [51-59] or PEO-based materials containing various salts [60-65]. A few studies have also been made using larger-scale modelling techniques on PFSA materials, like meso-scale modelling of the morphology of hydrated Nafion [66] and statistical mechanics modelling of Nafion pores [67]. The essential proton diffusion mechanism in PFSA materials is more complicated to model, since H-bond formation has to be included, but some attempts have been made using the two-state empirical valence-bond (EVB) model [68], the self-consistent multistate EVB (MS-EVB) model [69,70] or a reactive force field model [71].

The effect of side-chains

This thesis consists of the following four papers (**I**-**IV**), whose common denominator is the study of structural and dynamical changes in polymer electrolyte materials by adding and varying side-chain length and spacing:

- In Paper **I**, the effect on polymer dynamics by adding methoxy-terminated poly(ethylene oxide) (PEO) side-chains with different lengths and separations to an amorphous salt-free long-chain PEO backbone has been studied by Molecular Dynamics (MD) simulation at 293 K and 330 K.

- Paper **II** is a continuation of Paper **I** but with $LiPF_6$ salt-ions included. MD simulation techniques have been used to systematically investigate how the length and spacing of poly(ethylene oxide) (PEO) side-chains along a PEO backbone influence ion mobility for two different salt concentrations of $LiPF_6{\cdot}PEO_x$; x=10 and 30 at 293 K.

- Paper **III** provides a qualitative study of three PFSA materials where the side-chain length is varied from the shortest (in Dow/Hyflon) to Nafion to Aciplex. Both structural topology and dynamical processes of the ionomers have been evaluated at water concentrations equivalent to 5 and 15 H_2O molecules per sulphonate group. The simulation temperature is 293 K.

- Paper **IV** is a quantitative continuation of Paper **III** for larger simulation boxes. Here, Hyflon and Nafion were studied for a water concentration of 15 H_2O molecules per sulphonate group at 363 K.

Molecular Dynamics simulation

Overview

Molecular dynamics (MD) simulation is a computational realization of statistical mechanics. The technique is suitable for studying complex systems at equilibrium. Observation of dynamics in a molecular system in space and time gives considerable information about its structure and dynamical properties.

Simply expressed: in an MD simulation, a number of atoms are put into a simulation box and the interactions between the atoms are represented by classical forces. By repeatedly solving Newton's equations of motion, a "movie" is generated of the material in question. Electrons are not considered explicitly, but taken into account when developing the potentials of the *force-field* (FF) as input data to the simulation. The result of an MD simulation is intrinsically dependent on the FF, which needs to be of high accuracy for all possible interactions.

The force-field detail

The potential describing the long-range force field for the PEO chain in paper **I** and **II** has the form:

$$U(r) = A\exp\left(-\frac{r}{B}\right) - \frac{C}{r^6} + \frac{1}{4\pi\varepsilon_0}\frac{q_1 q_2}{r}. \qquad (1)$$

The first two terms represent the *Buckingham potential* (A, B and C are constants); the third term describes the electrostatic interaction, and r is the distance between two atoms. For PEO, the parameters A, B and C have been taken from Neyertz and co-authors [60,61]. The side-chain linkage-point torsional potential was developed by Hektor *et al.* [62] and is formulated as:

$$U_{tor}(\Phi) = u_0 + \sum_{k=1}^{3}\left[u_{2k-1}\cos(k\Phi) + u_{2k}\sin(k\Phi)\right] \qquad (2)$$

Paper **II** also makes use of the modified *Buckingham* and *Lennard-Jones* potentials to describe forces between polymer and $LiPF_6$ salts (constants taken from Borodin *et al.* [63]), and has the forms:

$$U(r) = A\exp\left(-\frac{r}{B}\right) - \frac{C}{r^6} - \frac{D}{r^4} + \frac{1}{4\pi\varepsilon_0}\frac{q_1 q_2}{r} \tag{3}$$

and

$$U(r) = \frac{A}{r^{12}} - \frac{B}{r^6} - \frac{C}{r^4} + \frac{1}{4\pi\varepsilon_0}\frac{q_1 q_2}{r} \tag{4}$$

respectively.

The former describes the intermolecular interactions between anions and between different parts of the polymer. The latter describes the bonds between anions and cations. All intramolecular potentials for salts are also taken from Borodin *et al.* [63], and for PEO from Neyertz *et al.* [60,61].

In Papers **III** and **IV**, which study PFSA materials, a FF has been used based on the work of Goddard III *et al.* [51] which, in turn, is based on the DREIDING force field [72] developed from DFT B3LYP calculations on gas-phase perfluoromethane. The flexible water potentials used in the simulations in this thesis were taken from Levitt *et al.* [73], which take bending effects into account.

Goddard III *et al.* [51] developed their FF specifically for Nafion, which meant that it had to be modified slightly for the other PFSA membranes. For Hyflon (or Dow), the side-chain potentials were taken from the description of the $–O–C–C–SO_3^-$ part of the Nafion side-chain, while the oxygen charge was reduced from −0.5416 to −0.4971 to maintain overall charge neutrality. For Aciplex, a charge-neutral CF_2-group – equivalent to the CF_2-groups in the backbone – was inserted between the last two -CF_2- groups in the original Nafion side-chain. All extra dihedral O-C-C-C and C-C-C-S angles were parameterized from DREIDING [72].

Initial structures and simulation detail

For both types of material studied in this thesis, preliminary studies have been made to probe which parameters are the most important. In this way, Paper **II** is a direct continuation of Paper **I**, and Paper **IV** a continuation of Paper **III**.

In Papers **I** and **II**, the examined polymer materials were branched PEO with backbones of 89-343 EO units to which 3, 6, 7, 8, 9 and 15 EO-unit side-chains were added. The selected spacings along the backbone between the PEO side-chains attachment points were 5, 10, 15, 20 and 50 EO-units.

The backbone and all side-chains were methoxy end-capped. Although two temperatures (293 K and 330 K) were applied in Paper **I**, only the lower one was chosen for the more thorough study in Paper **II** (including salt ions). This decreased the probability of ion pairing and clustering, and simulated the system at as realistic an operating temperature as possible. Whereas the aim of Paper **II** was to study the variation of polymer structure to find optimal conditions for ionic mobility/conductivity, the type of salt was of less relevance, so a common and widely used salt – $LiPF_6$ – was preferred.

When a salt is dissolved in a polymer matrix, the conductivity generally increases due to the addition of charge carriers. However, as the salt concentration is increased beyond a certain level, the conductivity is found to fall because of increased cross-linking and ion-pairing [8,12,38,74]. The conductivity maximum depends on salt, polymer structure and often temperature. Magistris *et al.* studied linear PEO-$LiPF_6$ systems in the salt concentration range of Li:EO ratio 1:100 to 1:12, and found the conductivity maximum to be at 1:30, independent of temperature [74]. However, Chung and Sohn [38] studied non-linear PEO materials with 3 EO-units long side-chains and found maximum conductivity in the Li:EO range 1:12 to 1:8. Therefore, salt ions at the two concentrations 1:10 and 1:30 were inserted into the 30 different polymer matrixes studied in Paper **I**. Reference systems without side-chains have also been simulated under the same conditions.

Papers **III** and **IV** comprise studies of PFSA membranes; the former article can be considered a preliminary study to Paper **IV.** Paper **III** investigates three PFSA-based materials with different side-chain lengths: starting from the shortest, Hyflon (also called Dow) to Nafion to Aciplex. In Paper **IV**, two of these – Hyflon and Nafion – are studied in more detail. The simulation time was then extend from 1 ns to 3 ns, and the simulation boxes made larger; ~75 Å cubic-box side length, which makes this one of the largest MD simulated PFSA materials using an all-atom force-field so far. In Paper **IV**, to enhance the probability of dynamic events, the simulation temperature was raised to a high yet realistic level for the MEA in its applications: 363 K. Water concentration was investigated in Paper **III** for 5 and 15 H_2O molecules per sulphonate group (*i.e.,* λ=5 and 15, respectively). As the purpose was to study side-chain effects on dynamics rather than water concentration, only one level of hydration (λ=15), common in PEMFCs, was chosen. The main purpose has been to compare several physical and chemical properties for varying side-chain length, try to cast light upon the fundamental mechanism of proton diffusion, contribute to experimental structural data regarding the hydrophobic and hydrophilic interface topology, their distribution over time and space, *etc*. It should be mentioned in this context, however, that the *Grotthuss* proton-jump mechanism is not included in the classical MD methodology.

All initial simulation boxes discussed in this thesis have been constructed by the MCGEN software [75], which grows the polymer chain sequentially; additional monomers are accepted or rejected based on an energetic algo-

rithm of Monte Carlo type. This generation of macromolecules into a fixed-size simulation box meets a fundamental problem: approaching a global energy minimum configuration at a realistic density takes unrealistically long time, especially when dealing with branched or cross-linked polymers. In order to accelerate the equilibration, a larger simulation box has been chosen with lower than the target density; the box-size decreased during the simulation.

Further simulation detail is given in the Appendix.

Analysis

Mean-Square-Displacements (MSDs), Radial Distribution Functions (RDFs) and Coordination Number Functions (CNFs) are basic tools used in this thesis for evaluating the statistics from MD in terms of dynamics and structure, respectively. The MSD is a measurement of the average distance travelled by atoms in a given time interval, while the RDF is a function that describes spherically averaged local organizations around any given atom or group of atoms as a function of the distance from these atoms. Integrating the area under the RDF up to the bond distance gives the coordination number, *i.e.,* the number of neighbouring atoms out to a given distance from the central point.

Two slightly different MSD methods have been used to evaluate either the diffusion coefficients of mobile species, for example, ions and water molecules, or the local mobilities of atoms in the polymer. The *time-averaged* MSD is a measurement of the average distance travelled by atoms. It is defined as:

$$\overline{\mathrm{MSD}}(t) = \left\langle \Delta \mathbf{r}_i(t)^2 \right\rangle = \left\langle \left(\mathbf{r}_i(t) - \mathbf{r}_i(0)\right)^2 \right\rangle \tag{5}$$

where $\mathbf{r}_i(t)$-$\mathbf{r}_i(0)$ is the (vector) distance travelled by the population of atoms of type *i* over a time interval *t*, and the square of the magnitude of this vector is averaged over many such time intervals. This quantity is often averaged over all molecules of a specific type. If the molecule encounters no molecular interactions, then the distance travelled will be proportional to the time interval - distance is velocity multiplied by time - and the MSD will increase quadratically with *t*. In denser phases, quadratic behaviour is seen only for a very short time interval; of the order of the mean collision time. Beyond this time, the motion of free particles is better described as a random walk, for which the MSD increases only linearly with time. The rate of growth of the MSD depends on how often the molecular collisions occur. At higher densities, it will take a longer time for a molecule to diffuse a given distance, as

other molecules continually hinder its progress. The limiting slope of the linear part of MSD(t) is related to the self-diffusion coefficient (*D*) by:

$$2dD = \lim_{t\to\infty} \frac{d}{dt} \left\langle \Delta \mathbf{r}_i(t)^2 \right\rangle \tag{6}$$

where *d* is the dimension of the space considered. The *time-averaged* MSD method was used widely in Papers **II**, **III** and **IV** to evaluate diffusion coefficients.

Non-averaged MSD is similar to time-averaged MSD, but is not averaged over several time intervals:

$$\mathrm{MSD(t)} = \Delta \mathbf{r}_i(t)^2 = \left(\mathbf{r}_i(t) - \mathbf{r}_i(0)\right)^2 \tag{7}$$

This function has been used in Papers **I, II** and **III** when estimating local mobility, since the polymer comprises a covalently bonded chain and is therefore not able to diffuse as a whole which, in turn, results in non-linear behaviour for the averaged MSD function.

The RDF, *g(r)*, which can be obtained either directly from diffraction experiments or calculated from MD simulations, is a function which describes the spherically averaged local organization around any given atom type. It thus gives the probability of finding a specific particle type at distance *r* from another particle type. If one counts the appearance of two species at separation *r* from $r = 0$ to $r = \infty$, one gets the radial distribution function *g(r)*. A few examples of radial distribution functions, calculated from a MD simulation, are shown in Paper **II**, Fig. 2.

The radial distribution function is a useful tool to describe the structure of a system. At short distances (less than the atomic diameter), *g(r)* is zero. This is due to the strong repulsive forces between the atoms, which make the probability of finding two atoms close to each other virtually zero. The first (and often largest) peak corresponds to the probability of finding two molecules at this specific separation distance. The RDF then falls and passes through a minimum value. At longer distances, *g(r)* approaches 1 if there is no long-range order. The area under a peak gives the effective coordination number for that particular shell of atoms. The integration of an RDF as a function of distance *r* gives a CNF, which gives the number of atoms at a certain distance from a given atom type.

In a solid, the radial distribution function has an infinite number of sharp peaks whose separations and heights are characteristics of the lattice structure. The mean-square-width of an RDF peak, σ^2, has ideally only a thermal disorder component σ_T^2 for crystals (resulting from thermal fluctuations in the bonds), while amorphous materials also have additional contributions resulting from topological disorder, σ_D^2 [76].

The definition of $g(r)$ implies that $\rho g(r) d\mathbf{r}$ is proportional to the probability of finding an atom in the volume element $d\mathbf{r}$ at a distance r from a given atom type, and (in three dimensions) $4\pi\rho g(r) r^2 \delta r$ is therefore the mean number of atoms in a shell of radius r and thickness δr surrounding the atom. To calculate the pair RDF from an MD simulation, the neighbours around each atom or molecule are sorted into distance intervals. The number of neighbours in each interval is then averaged over the entire simulation.

PEO-based materials

Structure

In Papers **I** and **II**, a special notations has been used to describe the system in terms of side-chain length, spacing and concentration, *e.g.,* 3-5_10 or 8-20_30. The first numbers (in the examples, "3-5" and "8-20") represent the length and spacing of the side-chains in EO units, respectively. The third denotes the salt concentration in the system, which in these examples are 1:10 or 1:30.

Polymer structure

After relaxing the simulation boxes, visual inspection of the branched PEO materials reveals helical PEO polymer backbones with more irregularly oriented side-chains attached to it. Figure 2 illustrates a snapshot of branched PEO material without salt ions, showing how one side-chain distorts the helical shape of a backbone, consequently decreasing the ordered structure; *i.e.,* suppressing crystallinity. The distribution of backbone −C−C−O−C− and −O−C−C−O− dihedral angles in salt-free materials, both with and without side-chains, exhibit *trans* and *gauche* dihedral angle conformations similarly to linear PEO materials [77], corresponding to the energy minima in the FF used. The major difference in polymeric structure between comb- and linear PEO is a slightly broader distribution of backbone dihedral angle values in the comb-material, indicating a higher flexibility.

Ion distribution

According to the RDF and CNF plots (examples for the 8-20_10 system are shown in Paper **II**, Fig. 2), cations are typically surrounded by ~5 oxygen atoms at distances 2.0-2.5 Å, while anions are surrounded by more irregular geometries with oxygen distances 5.5-6.0 Å. Both anions and cations are distributed more or less uniformly in all simulated systems, which can be seen from the high Li-Li and P-P distances. Ion pairing occurs, however, which is shown from the Li-P RDF at a distance of ~3.8 Å. The extent of ion pairing depends on salt concentration; it is higher in the 1:10 case.

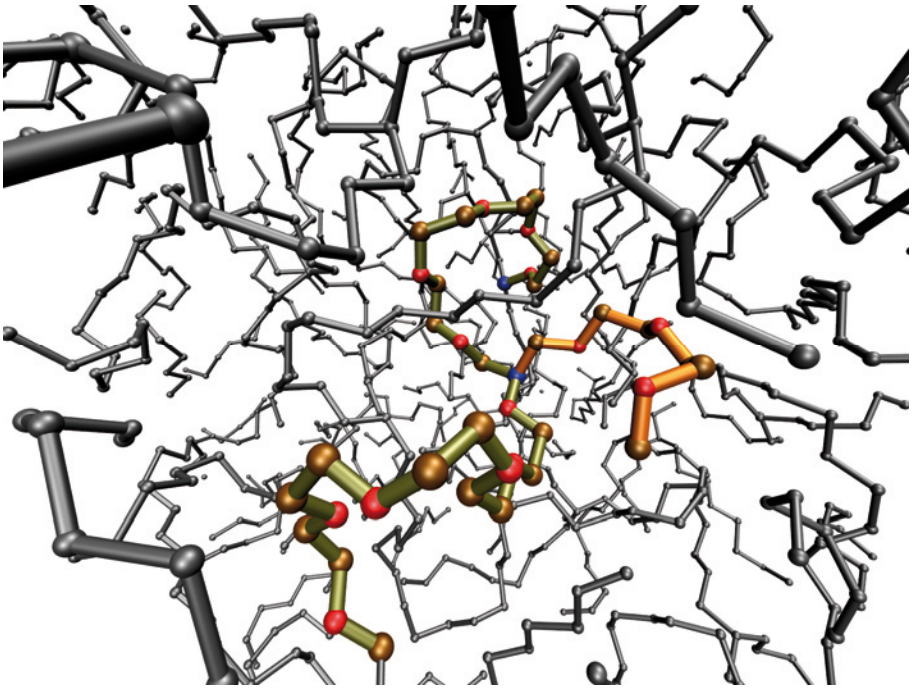

Figure 2. A snapshot of typical comb-shaped salt-free PEO at normal density. One 3 EO long side-chain (on the right side) and a fragment of the backbone is highlighted. The spacing between adjacent side-chains is 5 EO. For clarity, hydrogen atoms are omitted.

In Paper **II**, Fig. 3 gives an overview of the total ion-pairing (Li-P distances less than 4.5 Å) and -clustering in the simulated systems. At the higher concentration (Paper **II**, Fig. 3a), more than half of all atoms (between 68 % and 100 %) in each system participate in pair or cluster formation. Of these, more than 40% are in isolated pairs; few large clusters exist. At the lower concentration, the clusters are smaller, but also a lower proportion of the ions are involved in pair formation than at higher concentration: less than 33% in total in all simulated systems. In a few systems (6-10_30, 8-10_30 and 3-20_30), no ion pairing whatsoever is observed; all ions are thus completely dissolved into the PEO matrix.

Other MD studies [64] have shown that a major factor determining cation mobility is the behaviour of the side-chain ends. In Paper **II**, Fig. 5 shows how the cations are distributed in the PEO matrix; *i.e.,* whether they are coordinated to backbone or side-chains. Coordination to side-chains decreases with side-chain spacing, and increases with side-chain length; an effect of the molecular structure. To some extent, this trend reflects the fact that the distribution of side-chain and backbone atoms in the simulation boxes are different. Nevertheless, normalizing the results to the changing distribution of EO units displays the same trends; the dependence on side-chain separa-

tion is especially strong. This result indicates a *clear preference* for Li atoms to coordinate to the backbone, due to lower steric hindrance when the side-chains become more infrequent. When the side-chain separation is short, ions are less able to access the backbone, and are therefore located further out in the matrix.

Cross-linkage

It is well established [8] that cross-links are of major importance in determining both mechanical properties and ion conduction in polymer electrolytes. Linking polymer chains together leads to progressively larger branched polymers. Too much cross-linking can thus induce a high degree of rigidity, which would adversely affect ion mobility. The degree of cross-linking has a strong effect on the glass transition temperature.

A *cross-link* has in this thesis been defined as a cation bonded to different parts of the polymer matrix – pure chain-chain interactions are not considered. A distance of >2 uncoordinated EO units between coordinating ether oxygens has been selected to define such a cross-link. Figs. 6a and b in Paper **II** summarize the cross-linking. For some systems, the number of cross-links is even greater than the number of cations. In some local environments, a Li^+ ion can be involved in more than one type of cross-link; for example, it can connect two oxygen atoms from different parts of the backbone and, at the same time, two other oxygens from different parts of a side-chain.

It is clear that cross-linking increases at both concentrations both with increasing side-chain length and spacing, although this trend is weaker at the lower concentration and stronger for side-chain length than spacing. The cross-linkage increases with increasing side-chain length primarily because of a steady increase in the backbone-to-side-chain cross-links. Shorter side-chains do not extend far enough from the backbone into the polymer matrix to be able to participate in cross-linkage to other parts of the backbone; *i.e.*, polymer-chain entanglement is not as extensive. The overall increase in total cross-linkage with increased side-chain spacing (Paper **II**, Fig. 6b), on the other hand, is instead due to a sharply increasing level of backbone-to-backbone cross-linkage, which significantly outweighs the decrease in side-chain-to-side-chain cross-linkage. This is because the side-chains sterically hinder different parts of a backbone from connecting with one another; for increased spacing, this hindrance is diminished.

Mobility

Polymer mobility

It is the conventional wisdom [10-12] that side-chains raise the ion conductivity in PEO-based polymer electrolytes *mainly* through the suppression of crystallinity by breaking the long-range order. However, both PEO studies in Paper **I** and **II** confirm that, by adding short side-chains, the mobility of the amorphous polymer is also changed. To visualise variations in mobility, contour plots with *side-chain length* on the *x-axis* and *side-chain spacing* on the *y-axis* are used throughout the thesis; for example, in Figure 5.

The overall ether-oxygen mobility (including backbone and side-chain EO atoms) for the salt-free system, discussed in Paper **I**, is plotted for different side-chain lengths and separations and for both temperatures in Figure 3. At 293 K (Figure 3a), the clearest trend is that the overall EO mobility is relatively independent of side-chain separation; a mobility minimum (a trough) for side-chain lengths 6–7 EO-units and a mobility maximum (a ridge) for side-chain lengths of 9 EO units run almost parallel to one another. The situation at 330 K is more complicated (Figure 3b); we now see clear evidence of some chain-separation dependence, with the same peaks and troughs as at 293 K now diverging from a common overall mobility maximum (for a side-chain length of 9 EO-units and a separation of 10 EO-units). The mobility trough moves slowly to lower mobilities for lower side-chain lengths and higher side-chain separations, while the mobility maximum remains separation independent for roughly 10 EO-unit side-chains.

Not unexpectedly, the introduction of ions generally makes the polymer-host structure more rigid and less mobile (Paper **II**, Figs. 7 and 8). This is apparent from the different scale on the *z*-axis of the three contour plots; the maximum polymer mobility decreases from 4.9 $Å^2$/ns for the salt-free systems, to 1.46 $Å^2$/ns at low salt concentration and 1.24 $Å^2$/ns at high concentration. Not only does the introduction of salt generally decrease the overall polymer-host mobility, it also brings about some obvious changes in the mobility pattern with respect to salt-free systems.

High polymer mobility seems to coincide with configurations containing many short side-chains at higher concentration, while the situation is more complex at lower concentration. At least at the higher concentration, cross-linkage reduces polymer mobility, but is apparently not the only factor determining polymer mobility.

Fig. 9 in Paper **II** shows the overall polymer mobility, separated into side-chain and backbone components. In the same way as for salt-free systems, side-chain mobility is generally higher than backbone mobility, since the terminal groups can move around freely.

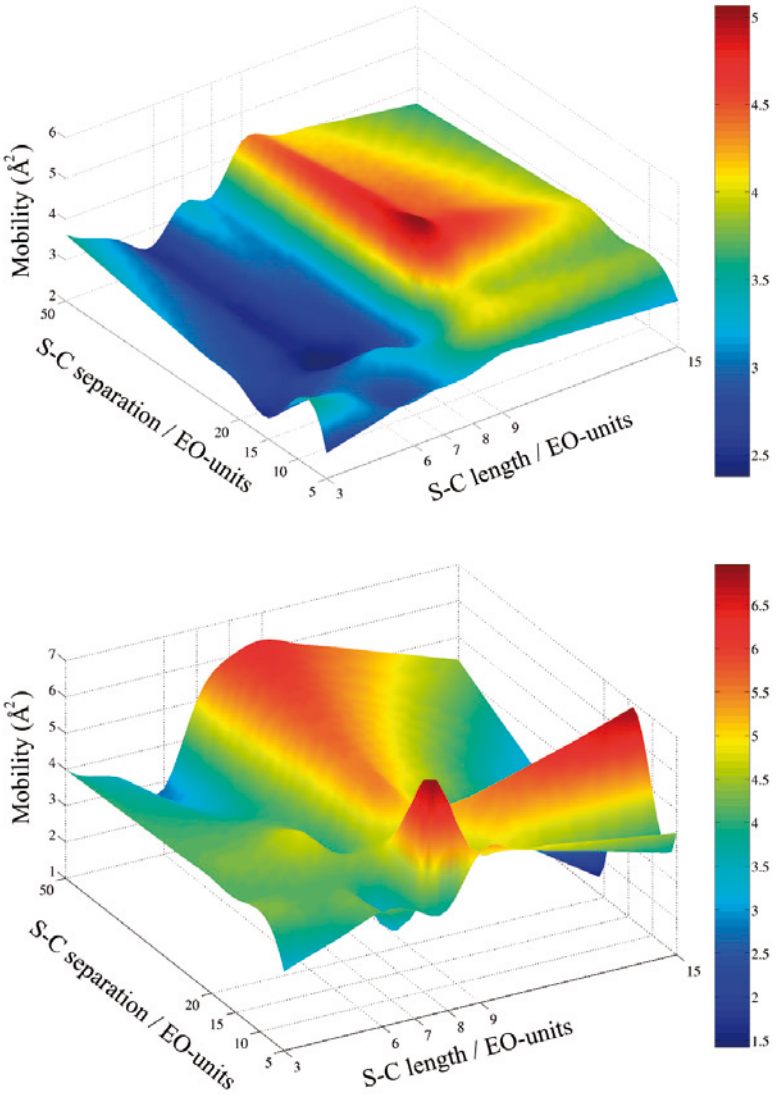

Figure 3. Overall ether-oxygen mobility (in $Å^2$/ns) taken over the whole system (including both backbone and side-chain atoms) for different side-chain lengths and separations at: (a) 293 K and (b) 330 K.

The mobilities of the backbone EO atoms would seem to be independent of where the side-chains are attached to the backbone. In other words, on the basis of ether-oxygen mobilities alone, it is not possible to identify the points of attachment of the side-chains. This trend was observed in both salt-containing and salt-free systems; see Fig. 10 in Paper **II**. However, the connecting point carbons tend to be among the least mobile atoms. The high mobility in certain sections of the backbone represents polymer segmental

motion, essential to Li^+ ion transport. That the connecting points participate less in this motion suggests a trade-off, with the more mobile side-chains promoting ion mobility, but at the same time slowing down backbone motion. Furthermore, the mobility for each EO atom along the side-chains shows an increasing trend towards the side-chain ends in both studies (see Fig. 4). Nevertheless, after salt has been inserted, the clear mobility maximum around 8-9 EO side-chain length (Fig. 4a and discussion in Paper **I**) disappeared (Fig. 4b) due to ion complexion involving side-chain ether-oxygen. The most mobile side-chain ends were still found in the range 7-8 EO units. Too long side-chains are less mobile, *i.e.*, they lose their side-chain identity and behave as the backbones.

Ion mobility

Figure 5 shows the Li-ion mobility for the two salt concentrations studied. The two figures (a and b) have slightly different z-scales, but their overall similarity would suggest that Li^+ mobility is not strongly dependent on concentration in the studied branched PEO systems, though slightly higher at lower concentration. The cation mobility values range from 0.5 to 1.2 $Å^2$/ns for the higher, and from 0.6 to 1.5 $Å^2$/ns for the lower concentration, compared to mobility values for the side-chain free reference systems of 0.66 and 0.81 $Å^2$/ns, respectively. The side-chain free systems display comparable values, but in the lower mobility region. Considering the substantial increase in number of charge carriers when the concentration increases from 1:30 to 1:10, the conductivity should be higher for the 1:10 than for the 1:30 systems. This is the contradictory to the experimental studies on linear PEO, where the maximum conductivity was found at concentration 1:30 [74], but agrees well with experimental conductivity values in comb-branched PEO materials, studied by Chung and Sohn [38]. The actual situation on a macroscale is complex, however, since PEO-based structures crystallize to a greater extent at higher concentrations at the simulation temperature 293 K, thereby depleting them of their charge carriers. Higher concentration also leads to a higher fraction of ions participating in pairs and clusters.

While cation and anion mobilities are similar for both ionic species, certain differences appear, however, in the polymer and cation mobilities. For example, in Paper **II**, Fig. 7b shows high polymer mobility for the 3-15_30 and 15-50_30 systems, which have no correspondence in the ion mobility (Figure 5b). This can be explained by the side-chains being responsible for the high overall mobility values; see Fig. 9b and 9d in Paper **II**. The ion distribution (Paper **II**, Fig. 5b) shows, on the other hand, that very few ions are located close to the side-chains in these particular systems.

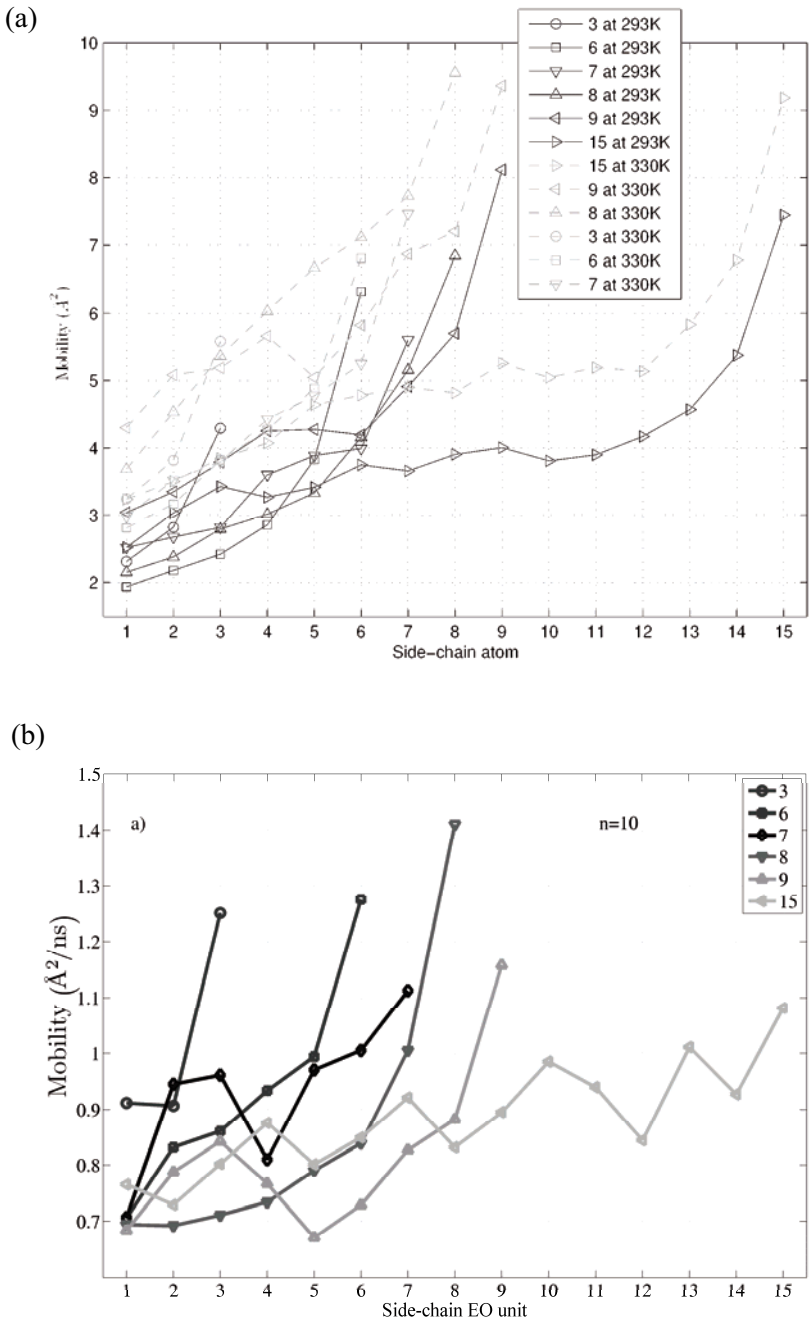

Figure 4. Variation in atomic mobility along the side-chains in: (a) salt-free PEO system and (b) $LiPF_6(PEO)_{10}$

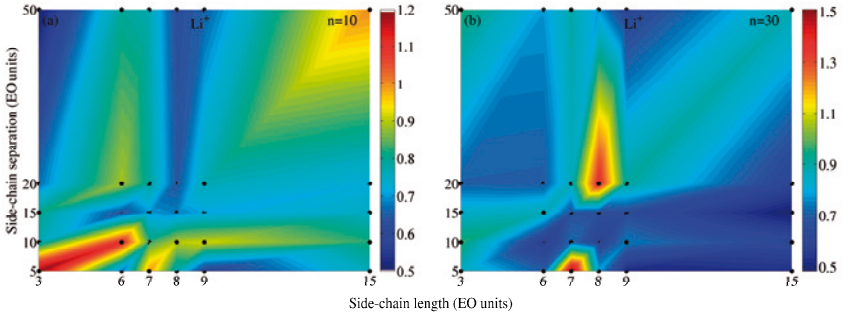

Figure 5. Li^+ mobilities (in $Å^2$/ns) in all simulated systems of $LiPF_6(PEO)_{10}$ (a) and $LiPF_6(PEO)_{30}$ (b).

Diffusion

Li^+ ion diffusion coefficients have been estimated from time-averaged MSD values; see also Fig. 13 in Paper **II**. Arumugam *et al.* [78] have measured diffusion coefficients experimentally for side-chain free $LiPF_6{\cdot}(PEO)_x$; for x values between 20 and 100. While they found diffusion coefficient (D_{Li+}) for Li^+ in the range $(0.20\text{-}0.25){\cdot}10^{-8}$ $cm^2{\cdot}s^{-1}$, the MD-derived values in Paper **II** are in the range $(0.25\text{-}3.36){\cdot}10^{-8}$ $cm^2{\cdot}s^{-1}$. This indicates that our results are realistic, considering that the experimental samples where not completely amorphous, and the studies were made for different concentrations.

Ion-jump mechanism

A jump-analysis of all ions shows that only a few ions in each system undergo longer jumps. At the higher concentration, the average distance travelled for all Li ions is 2.2(6) Å, while it is 2.4(6) Å at the lower concentration. Both these averaged values are slightly higher than for the side-chain free reference states (2.1(5) Å for both), but the nature of these jumps is so varied that these small differences are insignificant. However, side-chain free reference systems involve no ion-jumps of any significant distance during the simulations, which suggests that side-chains play some role in determining ion mobility mechanisms; they do not merely suppress crystallisation.

Four different types of cation motion were observed: intra-chain hopping, inter-chain hopping, intra-chain hopping *via* an ion cluster and inter-cluster hopping. These types of motion, discussed for example in [8], and are illustrated schematically in Figure 6. The inter-cluster hopping, where cation migration is assisted by anions, is also seen in Figure 7 (taken from one simulation). Furthermore, a Li^+ ion jump occurs either along or between side-chains and backbones, with no particular preference. This is contrary to what is found in side-chain free systems, where the cations predominantly move along the same backbone chain [63], *i.e.*, intra-chain hopping. The introduc-

tion of side-chains thus seems to add a dimension to the way Li^+ ions can move, which subsequently can lead to an increased overall mobility.

Interestingly, two different common types of local "ion traps" are seen around the most mobile Li^+ ions: the first involves a Li^+ ion at a side-chain-to-backbone connecting point, with both side-chain and backbone oxygens coordinating to the same Li^+ ion. The second occurs when two different PEO chains are cross-linked by a mobile Li-ion.

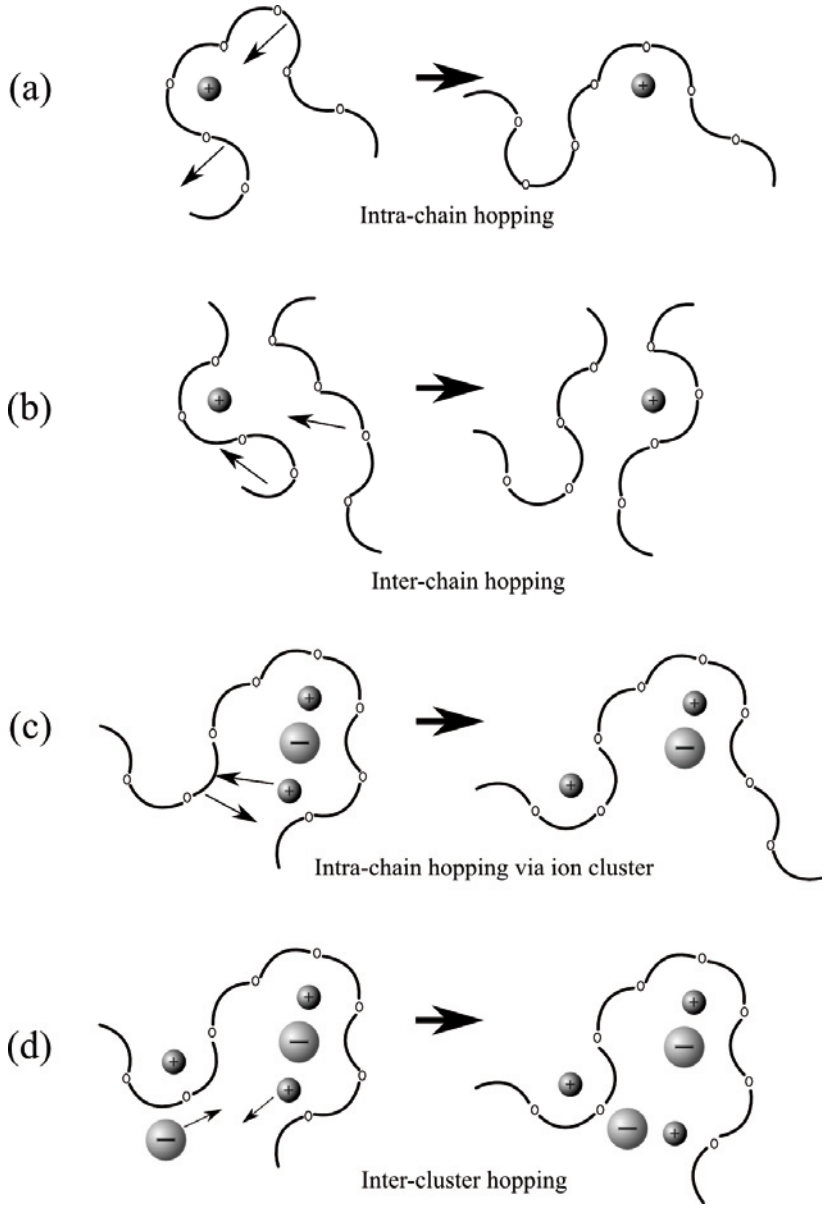

Figure 6. Possible cation motion mechanisms in a polymer electrolytes.

A quantitative analysis of individual cation jumps is summarized in Paper **II**, Tables 1 and 2. A total of 138 jumps occur at the higher concentration, and 50 at the lower concentration or, on average, 3.8 and 4.2 jumps per cation, respectively. However, the types of jump that dominate are different at the two concentrations. At the higher concentration, very few jumps occur for Li-ions coordinated to only one particular species (*i.e.,* intra-chain, inter-chain and inter-cluster hopping), *c.f.,* the upper left quadrant of Table 1 in Paper **II**. Most such jumps also occur between similar coordination types, *c.f.,* the main diagonal in Table 1. At the lower concentration (Table 2 in Paper **II**), more than one third of all jumps are intra-chain hopping along the backbone, resembling more a side-chain free system. More ion-pairing and cross-linking occur at higher concentration, thereby providing more possibilities for ions to find alternative transport routes through the polymer matrix by hopping *via* ion clusters. As expected, no jumps have been initiated from a coordination to anions only, *i.e.*, the electrostatic interaction is too strong to release any cations during the relatively short simulation time.

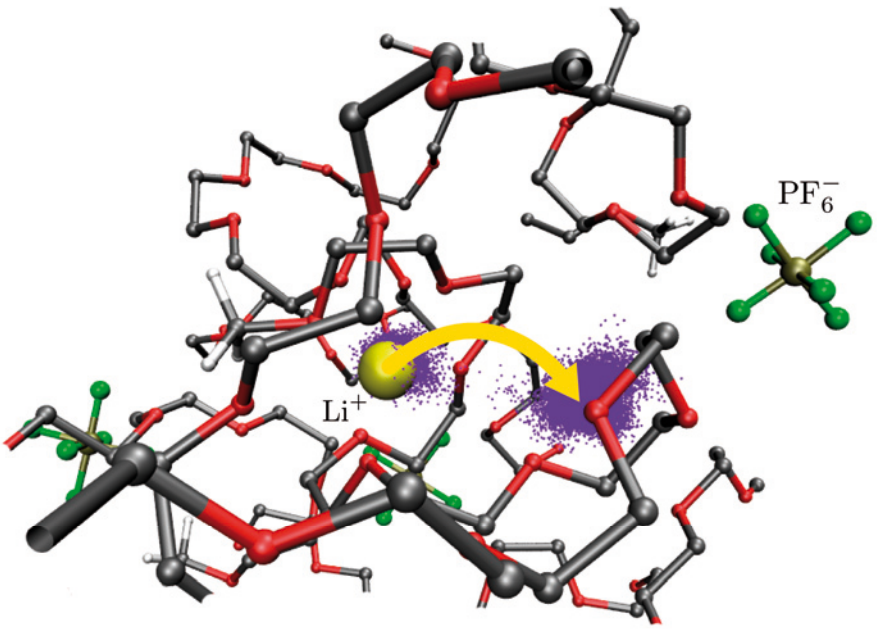

Figure 7. A typical Li^+ ion migration mechanism mediated by a PF_6^- anion in the comb-shaped polymer $LiPF_6(PEO)_{10}$ with side-chain lengths of 15 EO units and side-chain spacings of 50 EO units. The two clouds formed by small dots indicate the location of the Li^+ ion during the entire sampling time of the simulation.

PFSA-based materials

Similar to the PEO based electrolytes, the relationship between side-chain variations and material properties have also been studied for three PFSA materials – Hyflon/Dow, Nafion and Aciplex – at two water concentrations (λ=5 and 15) in Paper **III**. Two of these materials (Hyflon and Nafion) were studied further at λ=15 (a more realistic water content in FCs) using a larger simulation box in Paper **IV**.

Local structure

The local structures of the systems were also evaluated by RDFs and CNFs. The similarities in these curves between different materials indicated that the local structures close to the terminal SO_3^- groups and in the aqueous environment were rather independent of side-chain length. In other words, different side-chain lengths do not appear to result in significant differences in *local* structure. Only some marginal differences were seen: the number of SO_3^- groups in a sulphonate group cluster differs somewhat, and a slightly higher degree of hydration is seen around the sulphonate groups for longer side-chains, since they extend further into the water channels.

In Paper **III**, a set of different H-bond arrangements were observed in the H_3O^+/H_2O-sulphonate group regions. Some of these are typical of geometries in which a proton could be transferred from an H_3O^+ ion to a H_2O molecule, although this possibility has not been included in the calculations. With a hydrogen-bonding criterion of $d(H_{hydronium}...O_{water} < 1.9$ Å), many H_3O^+ protons are involved in H-bonds to either water molecules or sulphonate groups. Hydronium ions and H_2O molecules can also bridge different SO_3^- groups, and thereby form extended H-bonded networks (see Fig. 8).

As illustrated in Fig. 9, water molecules form an intermolecular hydrogen-bond network, and appear at typical H…O distances of 1.7-1.9 Å, and O-O distances of ~2.9 Å. The H_3O^+-H_2O RDFs show that one H_3O^+ is generally surrounded by 3-4 H_2O molecules at O-O distances of 2.8 Å.

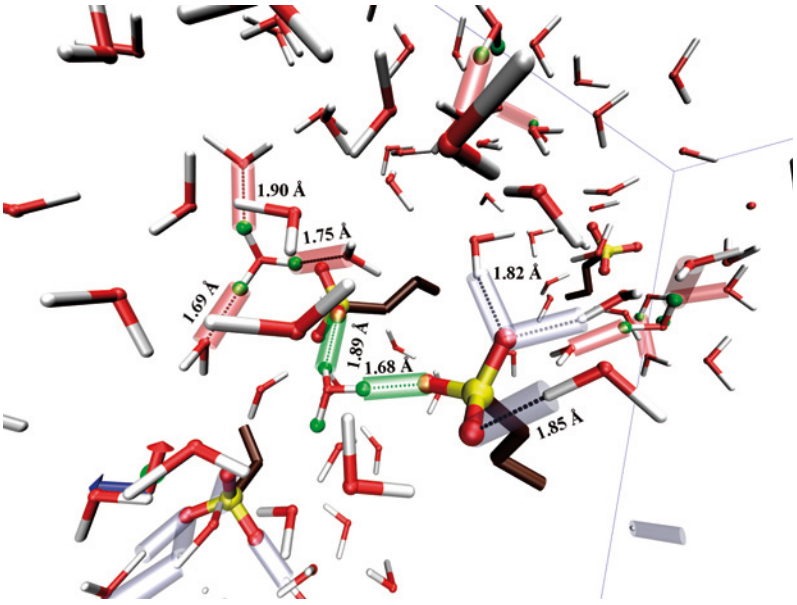

Figure 8. A typical example of the geometry of the H-bonded network involving H_3O^+/H_2O and SO_3 end-groups, taken from a typical snapshot of Nafion®, containing 15 water molecules per sulphonate group. Red cylinders indicate H_3O^+–H_2O bonds; green H_3O^+ – SO_3 bonds; and grey H_2O – SO_3 bonds. Only H-bond interactions for H…O distances <1.9 Å are highlighted.

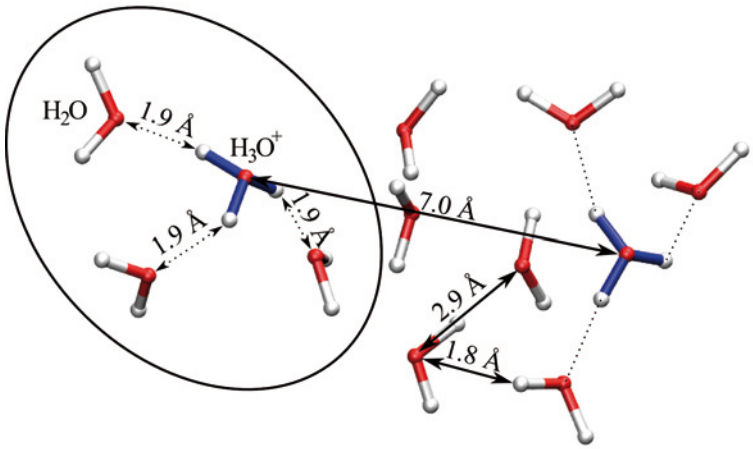

Figure 9. Typical local water/hydronium clustering in the H_2O/H_3O^+ channel in Nafion; a $H_9O_4^+$ ion is circled.

There are two distinct hydration spheres around the sulphonate groups, almost independent of polymer side-chain length. The first is at an S-O_W distance of ~4 Å, containing 5-7 water molecules; the second at ~6.3 Å. Although the water molecules are highly mobile, the water-hydrogens generally orient towards the oxygens of the SO_3^- groups with H_W–O_{SO3} hydrogen bond distances of 1.8 Å; as illustrated in Fig. 10.

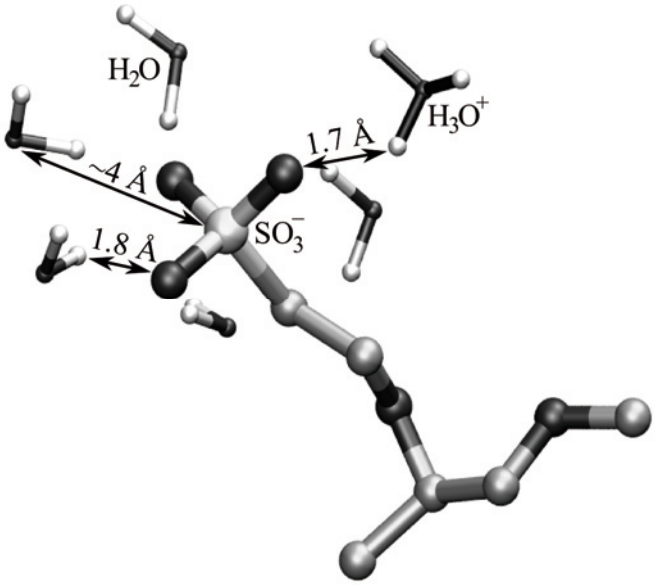

Figure 10. Local water/hydronium clustering around a sulphonate end-group in Nafion.

Fig. 11 shows the average distribution of such clusters for two different H…O length criteria: 1.7 Å and 1.9 Å. The similar distributions for the two systems are striking. When longer H…O distances are included in the analysis, both systems are dominated by $H_5O_2^+$ and $H_7O_3^+$ clusters; 75% of all H_3O^+ ions exist in these cluster types. Using the shorter H…O criterion, the systems are clearly dominated by H_3O^+ and $H_5O_2^+$ ions. The number of $H_5O_2^+$ ions does not change significantly with H…O distance criterion, indicating that $H_5O_2^+$ ions are reliably frequent occurrences.

As seen in Fig. 8, and in more detail in Fig. 12 (based on the S-S RDF), most side-chains aggregate in 3-4 SO_3^- group clusters with S-S-distances of 7-9 Å, with each SO_3^- group exhibiting one shorter S-S 7 Å distance. By counting side-chains which are closer to one another than 8 Å (corresponding to the first minimum of the S-S RDF plot), the average cluster size can be determined: 3.6 SO_3^- groups per cluster in Nafion, and 4.1 in Hyflon. At

any time-step, an average of 67 sulphonate-group clusters could be found in Nafion, and 61 in Hyflon. Hyflon thus promotes the formation of fewer but larger clusters than Nafion.

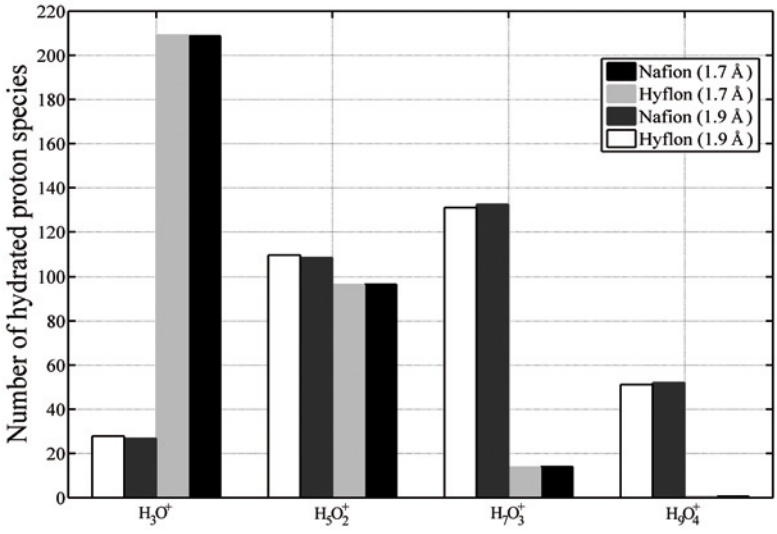

Figure 11. The average distribution of hydrated proton species in Nafion and Hyflon taken over all sampling timesteps for two H…O hydrogen-bond criteria: 1.7 Å and 1.9 Å.

However, not all side-chains participate in cluster formation: 24.6 % of all side-chains in Nafion, and 22.1 % in Hyflon are isolated side-chains distributed between the SO_3^- group clusters. The slightly larger number for Nafion could explain the experimental observation that the proton diffusion is roughly an order of magnitude higher in Nafion than in short side-chain PFSA polymers at low levels of hydration [43]. By gradually decreasing the water content in PFSA materials, the size and connectivity of the water channels also decreases. In Nafion, the single and separated side-chains can help maintain the connectivity of the remaining water channels at lower water content.

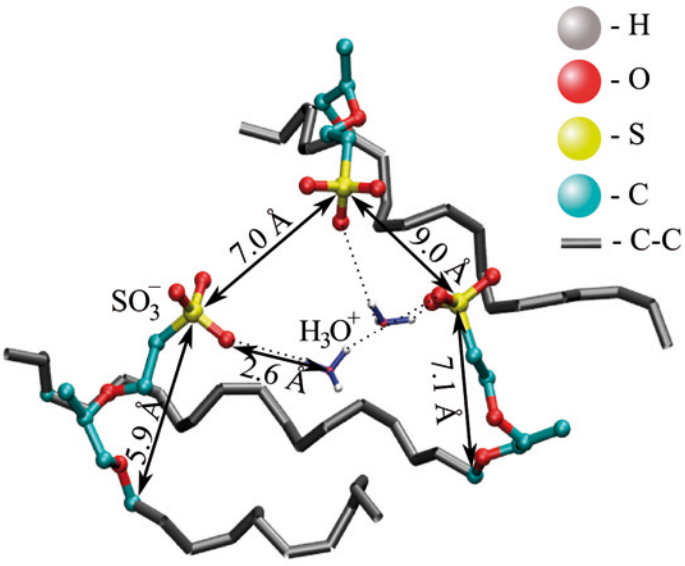

Figure 12. Hydronium-ion clusters linking different side-chains together in Nafion.

Nano-scale structure

All simulations in Papers **III** and **IV** clearly display formation of separate hydrophilic and hydrophobic phases. Water molecules and hydronium ions form a well-connected water-channel network, which is essential for the overall proton conductivity. The studies in Paper **III** also give insights into the dependence on water content; higher water content naturally raises both the connectivity and homogeneity of the water-channel network. Consequently, a smaller water content results in separated water domains and narrow water channels.

Fig. 9 in Paper **IV** illustrates the distribution of water-domain sizes found during the entire sampling time of the simulations. Two types of water cluster occur; some containing only a small numbers of water molecules, and others constituting large water domains/networks – no isolated water domain of intermediate size was found, nor did any of the large networks break up into smaller domains at any time; *i.e.,* the frequencies for the larger clusters sum to 100%. Although smaller clusters regularly break away from and rejoin the dominant larger network, the overall water-channel structure re-

mains stable and continuous in both materials throughout their entire simulation time. This is equally true for both Nafion and Hyflon.

Fig. 13 shows a 5 Å thick slice through the 76×76 Å Nafion simulation box, illustrating the spatial distribution of water, hydronium ions and sulphonate groups. Other atoms are not shown, so the polymer backbone appears as white regions, and the hydrophobic/hydrophilic interface is illustrated as a thick black line. The yellow clouds are the sulphonate clusters; the typical width of a water channel is around 10 Å. The SO_3^- groups are not situated directly on the channel surface, but extended somewhat into the aqueous regions. Although H_3O^+ ions can be found throughout the channel network, they clearly collect around the sulphonate groups.

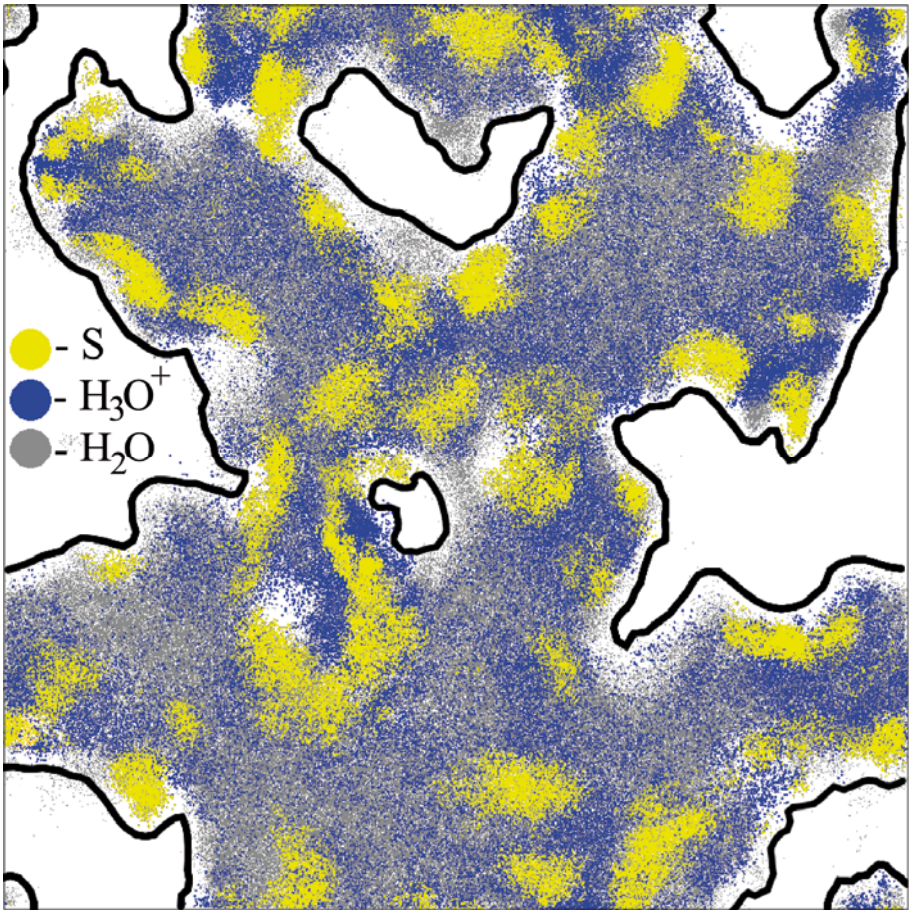

Figure 13. A 5 Å thick slice cut through Nafion. Empty regions represent the polymer, while the dots represent coordinates of different atom types during the simulation.

Figs. 14 and 15 shows histograms (plotted as curves) for H_2O and H_3O^+ distances to their closest polymer backbone atom; this gives an estimate of the topological character of the systems. The spatial distributions of the H_2O/H_3O^+ species show some noticeable differences. In Hyflon, both water molecules and hydronium ions are more frequent close to the polymer backbone. Considering that the number of water molecules is the same in both systems, this means that the polymer/water interface area is larger for Hyflon. Furthermore, since the number of polymer backbone atoms is the same for both polymers, it can be conclude that the surface-area to volume ratio (SAVR) is higher in Hyflon, which means that the water channel topology is less spherical than in Nafion. The polymer/water interface can be depicted as having a somewhat more tortuous form in Hyflon.

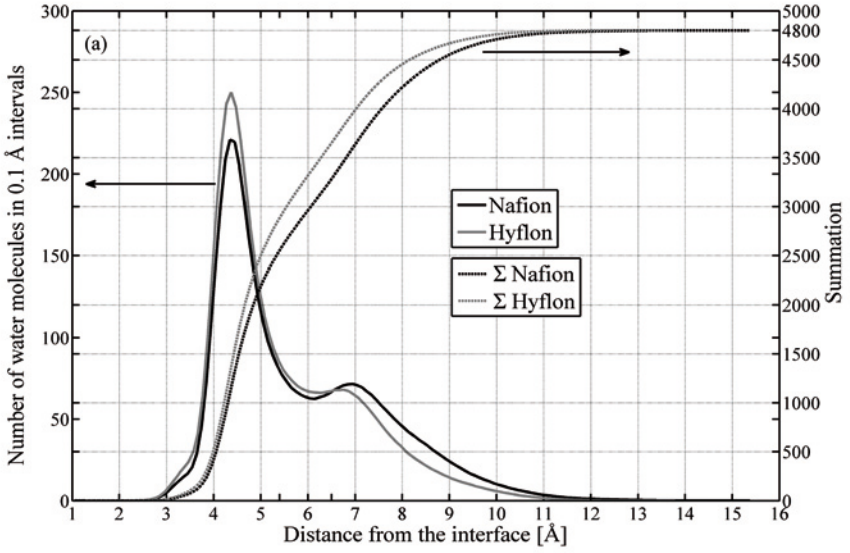

Figure 14. Histograms plotted as continuous curves of the closest distance between H_2O molecules and the polymer/water interface. The summation gives the number of molecules within a given distance from the polymer/water interface.

Table 3 in Paper **IV** gives the number of H_3O^+ ions as a function of distance from the polymer/water interface (Figs. 14 and 15). The thick horizontal line indicates the locations of the side-chain ends in the two cases. The spatial distribution of H_3O^+ ions at intermediate distances is clearly different; Hyflon has more loosely bonded and free H_3O^+ ions lying beyond its side-chain ends. It is these H_3O^+ ions, which are weakly associated with and thereby not immobilized by the SO_3^- end-groups. They are clearly prime contributors to proton transport in the system.

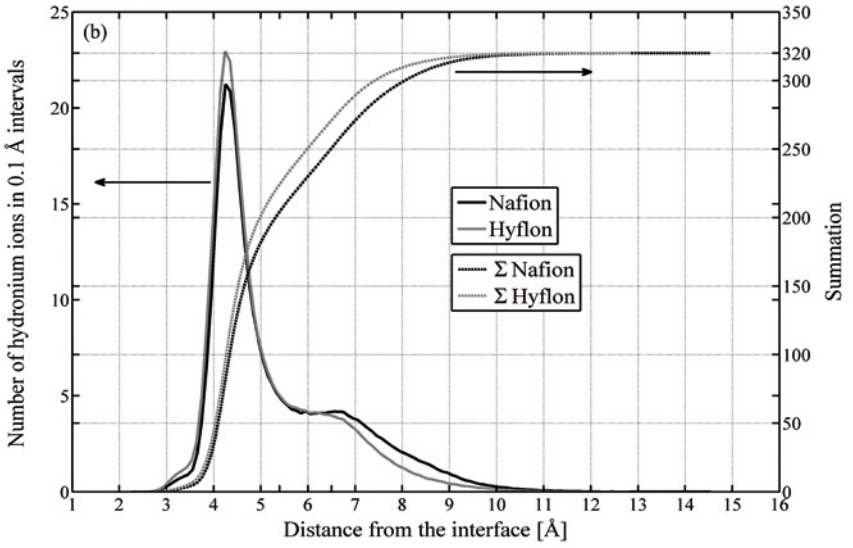

Figure 15. Histograms plotted as continuous curves of the closest distance between H_3O^+ ions and the polymer/water interface. The summation gives the number of molecules within a given distance from the polymer/water interface.

Dynamics

The MSD results in Paper **III** suggest that diffusion coefficients of H_3O^+ are expected to be larger in Nafion than in Hyflon or Aciplex, which also agrees well with the higher side-chain end mobility for Nafion at λ=15. This was one of the reasons for choosing Nafion for the extended study in Paper **IV**.

In the PEO studies (Papers **I** and **II**), it was found that the mobility of individual side-chain atoms increases along the side-chain towards the end-group, until a maximum is reached. When side-chains are elongated beyond this length, they lose their SC identity, and the mobility decreases. An equivalent observation could be made for the PFSA materials, since long side-chain Aciplex showed lower mobility than Nafion, probably also due to more interactions between the side-chains. Aciplex was therefore not included in Paper **IV**.

Mobility

In the context of fuel-cell applications, the "optimal" polymer configuration is the one with the highest proton conductivity. Therefore, the molecular speed and diffusion of H_3O^+ and H_2O are of prime importance. In Paper **III**, a qualitative approach showed that the most mobile species could be found

at the centre of the water channels. Fig. 16 (Paper **IV**) shows quantitatively how the drift speed of H_3O^+ ions and H_2O molecules in the cross-section of the water channels increases from the polymer/water interface to the centre. It is clear from both studies that hydronium ions are less mobile than water molecules. This difference is due to stronger electrostatic and hydrogen-bond interactions in which the hydronium ions participate. Shorter side-chains give higher speeds for both species beyond 4 Å, especially at the centre of the channels. Since the pendant side-chains tend to orient perpendicular to the hydrophilic/hydrophobic interface [55], long side-chains can restrain the dynamics further out in the hydrophilic environment.

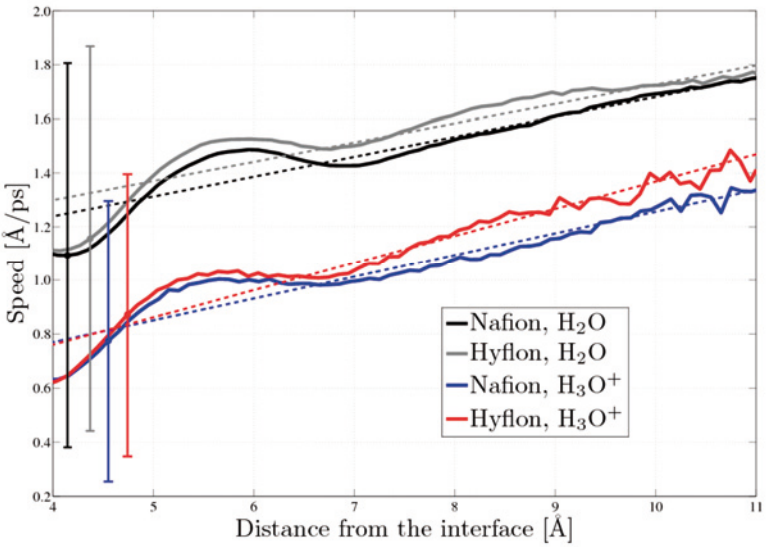

Figure 16. Mean molecular speeds for H_2O and H_3O^+ as a function of distance from the polymer/water interface. Standard deviations are shown as bars. The dashed lines are trendlines included as a guide for the eye.

Mean Residence Times (τ_{MRT}) have been calculated for H_2O/H_3O^+ around SO_3^- groups; these values show typically for how long (on average) an H_2O/H_3O^+ remains in the first coordination sphere around a chain-end; see Table 1. H_3O^+ is seen to have a roughly four times longer τ_{MRT} than H_2O around the sulphonate groups, as a result of the greater participation of H_3O^+ ions in hydrogen bonds. Interestingly, the H_2O and H_3O^+ τ_{MRT} values are 10 and 32 ps, respectively, greater in Hyflon than in Nafion. Hyflon would thus appear to have a more stable coordination sphere. This can be explained by the slightly increased hydration around the Nafion sulphonate groups, and that these H_2O molecules lie further away from the polymer/water interface; *i.e.*, the larger number of H_2O/H_3O^+ molecules around the SO_3^- groups increases the frequency of solvent molecule exchange.

Table 1. Mean residence times for H_2O (W) and H_3O^+ (H) around SO_3^- groups.

Interaction	Mean τ_{MRT} [ps]
Nafion, S-O_W	30.1
Hyflon, S-O_W	39.7
Nafion, S-O_H	138.8
Hyflon, S-O_H	171.4

Diffusion coefficients

In Nafion, the calculated water diffusion coefficient derived from our simulations (D_{H2O}) is $21.291(6)\cdot10^{-6}$ cm^2/s, while the hydronium diffusion coefficient (D_{H3O+}) is $6.150(4)\cdot10^{-6}$ cm^2/s. In Hyflon, the water diffusion coefficient (D_{H2O}) is $25.171(2)\cdot10^{-6}$ cm^2/s and the hydronium diffusion coefficient (D_{H3O+}) is $6.465(4)\cdot10^{-6}$ cm^2/s. For comparison, Perrin *et al.* [39] have measured the vehicular transport of H_3O^+ using quasi-elastic neutron scattering, and obtain a diffusion coefficient of $4\cdot10^{-6}$ cm^2/s, which is quite comparable with our MD values. Diffusion of hydronium ions is thus roughly 4 times slower than that for water molecules as a direct result of the stronger H_3O^+ involvement in hydrogen bonding. In addition, these diffusion coefficients are slightly higher in Hyflon: the differences are $3.9\cdot10^{-6}$ cm^2/s and $0.3\cdot10^{-6}$ cm^2/s for H_2O and H_3O^+, respectively. This can be a consequence of there being more H_3O^+ ions and H_2O molecules beyond the side-chain ends in Hyflon; also illustrated in Fig. 16.

Concluding remarks

This thesis discusses and demonstrates the fundamental relationships between the physical and chemical properties of battery and fuel-cell related polymer electrolyte materials and polymer side-chain structure and dynamics. However, PEO-based and PFSA-based materials are significantly different materials, both structurally and in terms of their charge transfer mechanisms. PFSA materials use a solvent (often water), in which the conductivity processes occur, while PEO-based electrolytes are themselves able to dissolve the charge carriers and are used dry. It is therefore hard to envision a common optimal side-chain configuration, viable for both of them, although such configurations may well exist for the material types individually.

Nevertheless, there exist some parallels between the two material types. The mechanism of charge transfer in PEO materials is based on continuous changes in coordination between ether-oxygen atoms and Li^+ ions, similar to the proton conduction mechanism in an aqueous environment, where protons coordinate to water-oxygen atoms. The main difference is that the PEO ether-oxygens are covalently bonded, while water and hydronium ions form a continuous hydrogen-bond network. In both cases, it is important to understand the behaviour of the host structures for the different charge carriers.

In this context, it has been possible to distinguish one common feature for PEO- and PFSA-based side-chain rich materials: an increase in mobility along the side-chain. All materials have displayed maximum mobility close to the side-chain ends while, on the other hand, too long side-chains are unfavourable for the overall side-chain mobility, mainly as a result of polymer entanglement.

In PEO-based electrolytes, the increased plasticity on a macroscopic scale and the mobility of the polymer chains by inclusion of short side-chains are important factors which enhance cation diffusion. This thesis supports the belief [64] that the highest mobility of cations is achieved when the ions are located close to the most mobile regions of the polymer; *i.e,* close to the end of side-chains. By varying the side-chain configuration, the mobility of the cations changes by a factor of 2-3 in the systems studied. At first sight, it would seem that a high salt concentration is preferred, since the product of charge carriers and their mobility is higher than at lower concentration. However, this result must be interpreted carefully since a high salt concentration also enhances the occurrence of ion-pairs, clusters and cross-links. At both concentrations, two particular systems display the highest cation mobil-

ity: at high concentration, systems with short side-chain lengths and spacing – 3-5_10 and 6-10_10; at lower concentration, side-chain configurations similar to the most mobile salt-free systems – 7-5_30 and 8-20_30. Based on the observation that the most mobile regions in a polymer matrix are the short side-chains, good ionic conductivity can be expected in a hypothetical material where the backbone does not attract cations, as occurs for short PEO-based side-chains.

The local structure in the different PFSA materials does not change much when the side-chain length is altered. Only a slightly higher hydration around the side-chain ends in Nafion could be observed, and the material has more isolated side-chains, which might maintain the continuity of the water channel also at lower levels of hydration. On the nano-scale, however, some noticeable differences were detected in the phase-separated structures: the Hyflon water channels have a more tortuous form, yet have a more stable continuous water network structure.

In the PFSA materials, the maximum hydronium diffusion is found in Hyflon – the material with shortest side-chain of those studied. This was found to be a consequence of the short side-chains giving comparatively more free H_3O^+ ions in the water channels beyond the sulphonate side-chain end-groups. The molecular speed of H_2O, H_3O^+ and other hydrated proton species were found to increase as a function of distance from the polymer/water interface.

Since only a few percent of the hydronium ions in Nafion and Hyflon are found in the high-mobility regions, it is tenuous to speculate as to which part of the hydrophilic H_2O/H_3O^+ domain contribute most to the overall proton diffusion: the high-speed regions containing few ions or the proton rich interface, where the H_3O^+ ions are immobilized by hydrogen bonds. To answer this question, a more complete model of the proton transfer must be added to the classical MD simulations: a challenging task for future studies.

Populärvetenskaplig sammanfattning

Den här avhandlingen behandlar två olika sorters material, vilka båda är relaterade till produktion och lagring av elektrisk energi. Det är svårt att överskatta betydelsen av detta forskningsområde, i synnerhet mot bakgrund av de problem omställningen av energisystemet för närvarande möter. Det är idag välkänt att stora åtgärder vidtas för att hitta alternativ till konventionella energikällor som olja och andra fossila bränslen. Dels finns risk för framtida resursbrist på dessa, och dels bidrar de till en problematisk miljöpåverkan, bland annat genom utsläpp av växthusgaser. För flera tillämpningar lämpar sig dock de alternativa energikällorna sämre och behöver kombineras med energilagring och energikonvertering. Att i större utsträckning använda bränsleceller och batterier är därför en viktig del av lösningen.

De material som främst diskuteras här kallas polyetylenoxid (PEO) och Nafion. De är olika sorters polymerer, det vill säga långa, kedjeliknande molekyler. Vidare är de jonledande elektrolyter: det förra materialet används i batterier, och det senare i lågtemperaturbränsleceller. Båda har använts i kommersiella produkter under en längre tid, men det finns fortfarande många aspekter att utforska och förbättra. Målet med forskningen i denna avhandling har varit att studera modifikationer av dessa material för att förbättra deras egenskaper, öka deras livslängd, och därmed indirekt göra batterier och bränsleceller billigare.

Även om den experimentella forskningen utgör naturvetenskapens bas, så är det ofta både dyrt och tidsödande att systematiskt syntetisera och modifiera långa serier av material i laboratorium. Under de senaste decennierna har därför datorsimuleringar i allt större utsträckning kompletterat laboratorieexperiment, och samtidigt vidgat vår förståelse och erbjudit nya perspektiv. Exempelvis är det idag möjligt att skapa en sig en bild av materialet på den atomära nivån, och baserat på denna konstruera matematiska modeller för att förutsäga lösningar på vetenskapliga problem. Studierna i denna avhandling inbegriper en av många tillgängliga beräkningstekniker – molekyldynamik (MD). Denna metod är användbar för att studera beteendet hos utvalda delar av material, innehållandes allt från ett fåtal molekyler till upp till hundratusentals atomer, under några nanosekunder. Detta är en mycket kort tidsperiod från vårt makroskopiska perspektiv, men ofta tillräckligt för att klarlägga trender på atomär nivå.

Det är välkänt att man kan påverka de dynamiska och strukturella egenskaperna hos ett polymert material genom att addera korta sidokedjor på

polymererna. I den här avhandlingen har de två ovan nämnda materialen modifierats genom sidokedjor av olika längd och/eller periodicitet. Med datorsimuleringar har sedan den ”optimala” kombinationen av sidokedjor för att stimulera mobilitet och transport hos de elektriska laddningsbärarna i materialen sökts. Mobiliteten hos litiumjoner i batterier, eller protoner i bränsleceller, är direkt kopplade till den effekt man får ut, liksom till andra vitala egenskaper. Även om de material som studerats är sinsemellan olika, kunde optimala sidokedjekonfigurationer för att generera maximal laddningsbärarmobilitet hittas för bägge materialtyperna. Vidare torde innehållet i denna avhandling bidra till den allmänna förståelsen av laddningstransport i polymerer, och hur korta sidokedjor på polymeren – påminnande om benen på en tusenfoting – påverkar den totala polymerstrukturens dynamik och beteende.

Acknowledgements

First of all, I would like to thank my supervisor Professor Josh Thomas for guidance and support during my time as a PhD student. Your exciting contributions to our scientific discussions and your constant enthusiasm have throughout kept me in the right balance between my computer calculations and the bigger scientific picture. You always had time to listen to me, guide me in the right direction and, not least, give linguistic feedback.

I also wish to thank my other supervisor, Dr. Daniel Brandell, for his unending patience with me during all the long hours we have been working together. I have really enjoyed the collaboration.

I also thank my third supervisor, Professor Alvo Aabloo at Tartu University in Estonia, who encouraged me throughout my studies, and first stimulated my interest to continue within a field of academic studies where I could use my IT knowledge.

To all persons at the Department of Materials Chemistry: thank you for contributing to a nice work atmosphere here!

I especially want to thank Anti and Katrin, who have helped me a lot. It was really great to be Anti's roommate, and I sincerely appreciate all opportunities to ask for help on my many problems during these years.

It was truly enjoyable to get to know and spend time with Tanguy and Emilie. Extraordinarily impressive were their constant efforts to do the impossible: teach me French!

Last but not least, I wish to send many grateful thoughts to my family, who throughout these years has supported me and accepted my far too frequent absence from Estonia. Tõesti suured tänud!

References

[1] "Key World Energy Statistics", International Energy Agency, 2008.
[2] W.S. Harris, *Electrochemical studies in cyclic esters*, University of California, Berkeley, 1958.
[3] W.V. Schalkwijk and B. Scrosati, *Advances in Lithium-Ion Batteries*, Springer, 2002.
[4] B.C.H. Steele, *Fast ion transport in solids: solid-state batteries and devices*, Elsevier, Amsterdam-London / New York, 1973.
[5] M. Lazzari and B. Scrosati, *Journal of The Electrochemical Society*, **127 (**1980) 773.
[6] D. Murphy, F. Di Salvo, J. Carides, and J. Waszczak, *Materials Research Bulletin*, **13 (**1978) 1395.
[7] A.M. Stephan, *European Polymer Journal*, **42** (2006) 21.
[8] F.M. Gray, *Polymer Electrolytes*, The Royal Society of Chemistry, UK, 1997.
[9] F. Croce, G.B. Appetecchi, L. Persi, and B. Scrosati, *Nature*, **394 (**1998) 456.
[10] M. Watanabe and A. Nishimoto, *Solid State Ionics*, **79** (1995) 306.
[11] L. Qi, Y. Lin, X. Jing, and F. Wang, *Solid State Ionics*, **139 (**2001) 293.
[12] A. Nishimoto, K. Agehara, N. Furuya, A.T. Watanabe, and M. Watanabe, *Macromolecules*, **32 (**1999) 1541.
[13] L. Gitelman, M. Israeli, A. Averbuch, M. Nathan, Z. Schuss, and D. Golodnitsky, *Journal of Computational Physics*, **227 (**2008) 8437.
[14] W. Vielstich, A. Lamm, and H. Gasteiger, *Handbook of Fuel Cells: Fundamentals, Technology, Applications*, Wiley, 2003.
[15] J. Larminie, *Fuel Cell Systems Explained,* SAE International, 2003.
[16] W. Grove, *Philosophical Magazine*, **14 (**1839) 127.
[17] M. Eikerling, A.A. Kornyshev, and A.R. Kucernak, *Physics Today*, **59** (2006) 38.
[18] K. Mauritz and R. Moore, *Chemical Reviews*, **104** (2004) 4535.
[19] R. Devanathan, *Energy & Environmental Science*, **1 (**2008) 101.
[20] O. Diat and G. Gebel, *Nature Materials*, **7** (2008) 13.
[21] K. Kreuer, S.J. Paddison, E. Spohr, and M. Schuster, *Chemical Reviews*, **104** (2004) 4637.
[22] M. Rikukawa and K. Sanui, *Progress in Polymer Science*, **25** (2000), 1463.
[23] M. Saito, N. Arimura, K. Hayamizu, and T. Okada, *Journal of Physical Chemistry B*, **108** (2004) 16064.
[24] N. Yoshida, T. Ishisaki, A. Watakabe, and M. Yoshitake, *Electrochimica Acta*, **43 (**1998) 3749.
[25] A. Ghielmi, P. Vaccarono, C. Troglia, and V. Arcella, *Journal of Power Sources*, **145** (2005) 108.

[26] V. Arcella, A. Ghielmi, and G. Tommasi, *Annals of the New York Academy of Sciences*, **984** (2003) 226.
[27] G. Gebel and R. Moore, *Macromolecules*, **33** (2000) 4850.
[28] R.B.I. Moore and C.R. Martin, *Macromolecules*, **22** (1989) 3594.
[29] L. Merlo, A. Ghielmi, L. Cirillo, M. Gebert, and V. Arcella, *Separation Science and Technology*, **42** (2007) 2891.
[30] L. Merlo, A. Ghielmi, L. Cirillo, M. Gebert, and V. Arcella, *Journal of Power Sources*, **171** (2007) 140.
[31] P.V. Wright, *British Polymer Journal*, **7** (1975) 319.
[32] Y.G. Andreev and P.G. Bruce, *Journal of Physics: Condensed Matter*, **13** (2001) 8245.
[33] Y.G. Andreev and P.G. Bruce, *Electrochimica Acta*, **45** (2000) 1417.
[34] C. Berthier, W. Gorecki, M. Minier, M. Armand, J. Chabagno, and P. Rigaud, *Solid State Ionics*, **11** (1983) 91.
[35] K. Motogami, M. Kono, S. Mori, M. Watanabe, and N. Ogata, *Electrochimica Acta*, **37** (1992) 1725.
[36] A. Nishimoto, M. Watanabe, Y. Ikeda, and S. Kohjiya, *Electrochimica Acta*, **43** (1998) 1177.
[37] Y. Ikeda, Y. Wada, Y. Matoba, S. Murakami, and S. Kohjiya, *Electrochimica Acta*, **45** (2000) 1167.
[38] J. Chung and H. Sohn, *Journal of Power Sources*, **112** (2002) 671.
[39] J. Perrin, S. Lyonnard, and F. Volino, *Journal of Physical Chemistry C*, **111** (2007) 3393.
[40] W.Y. Hsu and T.D. Gierke, *Journal of Membrane Science*, **13** (1983) 307.
[41] K. Schmidt-Rohr and Q. Chen, *Nature Materials*, **7** (2008) 75.
[42] V. Arcella, C. Troglia, and A. Ghielmi, *Industrial and Engineering Chemistry Research*, **44 (**2005) 7646.
[43] K. Kreuer, M. Schuster, B. Obliers, O. Diat, U. Traub, A. Fuchs, U. Klock, S. Paddison, and J. Maier, *Journal of Power Sources*, **178 (**2008) 499.
[44] A. Arico', V. Baglio, A. Di Blasi, V. Antonucci, L. Cirillo, A. Ghielmi, and V. Arcella, *Desalination*, **199** (2006) 271.
[45] W. Schmittinger and A. Vahidi, *Journal of Power Sources*, **180** (2008) 1.
[46] T. Schlick, *Molecular Modeling and Simulation*, Springer, 2002.
[47] A. Leach, *Molecular Modelling: Principles and Applications*, Prentice Hall, 2001.
[48] D. Frenkel, D. Frenkel, and B. Smit, *Understanding Molecular Simulation*, Academic Press, 2001.
[49] S. Paddison and J. Elliott, *Journal of Physical Chemistry A*, **109** (2005) 7583.
[50] S.J. Paddison, *Annual Review of Materials Research*, **33** (2003) 289.
[51] S. Jang, V. Molinero, T. Cagin, and W. Goddard III, *Journal of Physical Chemistry B*, **108** (2004) 3149.
[52] R. Devanathan, A. Venkatnathan, and M. Dupuis, *Journal of Physical Chemistry B*, **111** (2007) 8069.
[53] S. Cui, J. Liu, M. Selvan, D. Keffer, B. Edwards, and W. Steele, *Journal of Physical Chemistry B*, **111 (**2007) 2208.

[54] J.A. Elliott, S. Hanna, A.M.S. Elliott, and G.E. Cooley, *Physical Chemistry Chemical Physics*, **1** (1999) 4855.
[55] S. Urata, J. Irisawa, A. Takada, W. Shinoda, S. Tsuzuki, and M. Mikami, *Journal of Physical Chemistry B*, **109** (2005) 4269.
[56] N. Blake, G. Mills, and H. Metiu, *Journal of Physical Chemistry B*, **111 (**2007) 2490.
[57] R. Devanathan, A. Venkatnathan, and M. Dupuis, *Journal of Physical Chemistry B*, **111** (2007) 13006.
[58] A. Venkatnathan, R. Devanathan, and M. Dupuis, *Journal of Physical Chemistry B*, **111** (2007) 7234.
[59] A. Vishnyakov and A.V. Neimark, *Journal of Physical Chemistry B*, **105** (2001) 9586.
[60] S. Neyertz, D. Brown, and J.O. Thomas, *The Journal of Chemical Physics*, **101** (1994) 10064.
[61] A. Aabloo and J.O. Thomas, *Computational and Theoretical Polymer Science*, **7** (1997) 47.
[62] A. Hektor, M.K. Klintenberg, A. Aabloo, and J.O. Thomas, *Journal of Materials Chemistry*, **13** (2003) 214.
[63] O. Borodin and G. Smith, *Macromolecules*, **39** (2006) 1620.
[64] O. Borodin and G. Smith, *Macromolecules*, **40** (2007) 1252.
[65] O. Borodin, G. Smith, and R. Jaffe, *Journal of Computational Chemistry*, **22** (2001) 641.
[66] J. Wescott, Yue Qi, L. Subramanian, and T. Capehart, *Journal of Chemical Physics*, **124** (2006) 134702.
[67] R. Paul and S.J. Paddison, *The Journal of Chemical Physics*, **123** (2005) 224704.
[68] E. Spohr, *Molecular Simulation*, **30** (2004) 107.
[69] M. Petersen, F. Wang, N. Blake, H. Metiu, and G. Voth, *Journal of Physical Chemistry B*, **109** (2005) 3727.
[70] M. Petersen and G. Voth, *Journal of Physical Chemistry B*, **110** (2006) 18594.
[71] Hofmann, Kuleshova, and D'Aguanno, *Journal of Molecular Modeling*, **14** (2008) 225.
[72] S. Mayo, B. Olafson, and W. Goddard, *Journal of Physical Chemistry*, **94** (1990) 8897.
[73] M. Levitt, M. Hirshberg, R. Sharon, K. Laidig, and V. Daggett, *Journal of Physical Chemistry B*, **101** (1997) 5051.
[74] A. Magistris, P. Mustarelli, E. Quartarone, and C. Tomasi, *Solid State Ionics*, **136-137** (2000) 1241.
[75] E. Soolo, J. Karo, H. Kasemägi, M. Kruusmaa, and A. Aabloo, *Smart Structures and Materials 2006: Electroactive Polymer Actuators and Devices (EAPAD)*, San Diego, USA: SPIE, (2006) 61682A.
[76] S.R. Elliott, *Physics of amorphous materials*, Longman, 1990.
[77] P.J. Flory, *Statistical Mechanics of Chain Molecules*, Hanser Publishers, 1989.
[78] S. Arumugam, J. Shi, D. Tunstall, and C. Vincent, *Journal of Physics:Condensed Matter*, **5** (1993) 153.

Appendix

Technical simulation details:

Paper **I**:

- A total of 62 different models were simulated:
  - 6 different side-chain lengths, comprising 3, 6, 7, 8, 9, 15 EO units
  - 5 different side-chain separations of 5, 10, 15, 20 and 50 EO units
  - 2 PEO reference systems without side-chains
  - 2 different temperatures: 293 K and 330 K
- Each MD simulation box-size was stable at ca. 28×28×28 Å
- Normal pressure (1 bar)
- The effective density was maintained at ca. 1 g/cm^3
- Boundary conditions; Ewald summation (cut-off: 13 Å)
- Simulation time-step: 0.5 fs
- Equilibration steps: 150 ps followed by 300ps in NVT
- Simulation time: 1 ns in NPT at both temperature levels
- Data were collected after every 0.5 ps

Paper **II**:

- A total of 62 different models were simulated:
  - 6 different side-chain lengths, comprising 3, 6, 7, 8, 9, 15 EO units
  - 5 different side-chain separations of 5, 10, 15, 20 and 50 EO units
  - 2 different salt concentrations: $LiPF_6{\cdot}PEO_{10}$ and $LiPF_6{\cdot}PEO_{30}$
  - 2 side-chain-free reference systems, one for each concentration.
- Each MD simulation box-size was stable at ca. 29×29×29 Å
- Simulation temperature: 293 K
- Normal pressure (1 bar)
- The densities for the side-chain free reference systems:
  - for the salt-free systems: 1.13 g/cm^3
  - for the higher salt concentration: 1.39 g/cm^3
  - for the lower salt concentration: 1.24 g/cm^3
- The average effective densities for systems with side-chains:
  - for the higher salt concentration: 1.40 g/cm^3
  - for the lower salt concentration: 1.23 g/cm^3
- Boundary conditions; Ewald summation (cut-off: 14 Å)
- Simulation time-step: 1 fs

- Equilibration steps: 30 ps annealing in NPT at 2000 K, followed by 50 ps quenching to 293 K, followed by salt insertion, tethered for the next 50 ps in NPT, followed by 0.8 ns in NPT
- Simulation time: 2.2 ns in NPT
- Data were collected after every 0.1 ps

Paper **III**:

- Three different materials studied: Dow®/Hyflon®, Nafion®, Aciplex®
- 4 different oligomers, each of them with 10 side-chains
- Water content: $\lambda = 5$ and 15
- Each MD simulation box-size was stable at ca. 40×40×40 Å
- Simulation temperature: 293 K
- Normal pressure (1 bar)
- Boundary conditions; Ewald summation (cut-off: 16 Å)
- Simulation time-step: 1 fs
- Equilibration steps: 100 ps in NVE followed by 500 ps NPT
- Simulation time: 1 ns in NPT
- Data were collected after every 1 ps

Paper **IV**:

- Two different materials studied: Nafion®, Hyflon®/Dow®
- 32 different oligomers, each of them with 10 side-chains
- Water content: $\lambda = 15$; *i.e.,* 4800 H_2O, 320 H_3O^+
- Each MD simulation box-size was stable at ca. 74×74×74 Å
- Simulation temperature: 363 K
- Normal pressure (1 bar)
- Boundary conditions; Ewald summation (cut-off: 20 Å)
- Simulation time-step: 1 fs
- Equilibration steps:
  - Nafion: 5 ps in NVT at 363 K, followed by 0.5 ns in NPT
  - Hyflon: 40 ps in NVT at 363 K, followed by 500 ps in NPT at 423 K
- Simulation time: 3 ns in NPT
- Data were collected after every 0.5 ps

Acta Universitatis Upsaliensis

Digital Comprehensive Summaries of Uppsala Dissertations from the Faculty of Science and Technology 635

Editor: The Dean of the Faculty of Science and Technology

A doctoral dissertation from the Faculty of Science and Technology, Uppsala University, is usually a summary of a number of papers. A few copies of the complete dissertation are kept at major Swedish research libraries, while the summary alone is distributed internationally through the series Digital Comprehensive Summaries of Uppsala Dissertations from the Faculty of Science and Technology. (Prior to January, 2005, the series was published under the title "Comprehensive Summaries of Uppsala Dissertations from the Faculty of Science and Technology".)

Distribution: publications.uu.se
urn:nbn:se:uu:diva-100738

ACTA
UNIVERSITATIS
UPSALIENSIS
UPPSALA
2009